THE EFFECT OF T-SHAPED FIN GEOMETRIES ON HEAT TRANSFER RATE ENHANCEMENT

A Thesis Submitted to
the Graduate School of Engineering and Sciences of
Izmir Institute of Technology
in Partial Fulfillment of the Requirements for the Degree of

MASTER OF SCIENCE

in Mechanical Engineering

by
Eylem ÇETİN

July, 2017
IZMIR

We approve thesis of **Eylem ÇETİN**

Examining Committee Members:

_____

Assoc. Prof. Dr. Erdal ÇETKİN
Department of Mechanical Engineering, Izmir Institute of Technology.

_____

Assist. Prof. Dr. Murat BARIŞIK
Department of Mechanical Engineering, Izmir Institute of Technology.

_____

Assist. Prof. Dr. Sercan ACARER
Department of Mechanical Engineering, Izmir Katip Celebi University.

13 July 2017

_____

Assoc. Prof. Dr. Erdal ÇETKİN
Supervisor, Department of
Mechanical Engineering Izmir
Institute of Technology

_____

Prof. Dr. Metin TANOĞLU
Head of the Department of Mechanical
Engineering

_____

Prof. Dr. Aysun SOFUOĞLU
Dean of the Graduate School
of Engineering and Sciences

ACKNOWLEDGMENTS

I would like to express my appreciation to my advisor Dr. Erdal ÇETKİN for his supervision.

I also would like to appreciate my colleagues Faruk TUNA and Awais AHMAD for their support and friendship. Their support made my life better.

In the end, I would like to thank my parents for their support, patience and love. Their presence always makes me stronger.

ABSTRACT

THE EFFECT OF T-SHAPED FIN GEOMETRIES ON HEAT TRANSFER RATE ENHANCEMENT

In this study, we show that maximum excess temperature on a heat generating cylindrical solid domain can be minimized with numerically optimized rectangular cavities and T-shaped fins. The effects of the cavities and the fins on heat transfer rate enhancement were compared while their volume fractions in a unit volume element were fixed. Furthermore, the designs correspond to the minimum thermal resistance were uncovered for two types of flows; parallel and cross-flow. The governing equations of the heat transfer and the fluid flow were solved simultaneously in order to show the effects of flow characteristics and the design on the thermal performance.

Two-dimensional solution domain was used to uncover the thermal performance in cross-flow case. Because the flow direction is perpendicular to the heat transfer surface area of the heat generating domain. However, three-dimensional domain was used in parallel flow case because the fluid flows along the outer surface of the heat generating domain and the heat transfer surface area. For the cross-flow case, the results show that T-shaped assembly of fins with longer stem and shorter tributaries corresponds to the lower peak temperature. In addition, the results also show that there is an optimal cavity shape that minimizes the peak temperature. This optimal shape becomes thinner when the number of the cavities increase. In parallel flow case, fins with thicker and shorter stem and longer tributaries corresponds to the minimum excess temperature. In addition, long and thin cavity shapes increase the thermal performance in parallel flow case.

ÖZET

T ŞEKİLLİ KANAT GEOMETRİLERİNİN ISI TRANSFER ORANI ARTTIRIMINDAKİ ETKİLERİ

Bu çalışmada ısı üretimli silindirik bir katı bölgede biriken maksimum sıcaklığın sayısal olarak optimize edilmiş dikdörtgen kaviteler ve T şekilli kanat montajı ile minimize edilebileceği gösterilmektedir. Kavite ve kanatların ısı transfer oranı arttırımındaki etkileri birim hacim içindeki oranları sabit tutularak karşılaştırılmıştır. Ayrıca parallel ve zıt akış olarak iki tip akış tipinde minimum ısıl direnc elde edilen tasarımlar bulunmuştur. Isı transferi ve akış denklemleri, akış karakteristiği ve tasarımdaki değişimlerin performans üzerindeki etkilerini göstermek için eşzamanlı olarak çözülmüştür.

Zıt akış durumunda, akışın ısı üretimli bölgenin ısı tansferinin gerçekleştiği yüzey alanına dik gelmesinden dolayı çözümlemeler 2 boyutlu model üzerinde yapılırken, paralel akışlı durumda ise akışkan hareketinin ısı üretimli bölgenin dış yüzeyi ve toplam ısı transfer yüzey alanı boyunca olmasından dolayı 3 boyutlu model üzerinde yapılmıştır. Zıt akışlı durumda, daha düşük maksimum sıcaklığa sahip kanat tasarımlarının uzun saplı ve kısa dallanmalı olduğu sonucuna ulaşılmıştır. Ayrıca, yapılan analizler termal performansı daha iyi olan optimum bir kavite geometrisinin olduğunu göstermektedir. Bu kavite geometrisi kavite sayısı arttıkça daha dar bir yapıya bürünmektedir. Paralel akışlı durumda ise daha kalın ve kısa saplı, uzun dallanmalı kanat tasarımları ısıl direnci düşürmekte iken kavite modellerinde bu durum daha uzun ve ince kavite tasarımları ile sağlanmaktadır.

TABLE OF CONTENTS

LIST OF FIGURES

Figure **Page**

LIST OF TABLES

Table **Page**

LIST OF SYMBOLS

R	Radius of the cylinder [m]
T	Temperature [K]
N	Number of the fins and/or cavities
A	Area of the cylindrical solid domain of size [m^2]
A_{cv}	Total cavity area [m^2]
L_0	Length of the one tributary [m]
t_0	Thickness of the tributaries [m]
L_1	Length of the stem [m]
t_1	Thickness of the stem [m]
H_f	Height of the fluid domain [m]
L_f	Length of the fluid domain [m]
W	width [m]
K	thermal conductivity [$Wm^{-1}K^{-1}$]
$\tilde{k}_I$	Conductivity ratio of the fin and heat generating domain (k_t/k_c)
$\tilde{k}_{II}$	Conductivity ratio of the fluid and the fin (k_f/k_t)
$\tilde{k}_{III}$	Conductivity ratio of the fluid and heat generating domain (k_f/k_c)
q'''	Heat source [Wm^{-3}]
x, y, z	Spatial coordinates [m]
u, v, w	Velocity components corresponding to the spatial coordinates [m/s]
c_p	Specific heat at constant pressure [J/kgK]

Greek Letters

ρ	Density [kg/m^3]
ν	Kinematic viscosity [m^2/s]
ϕ_t	Volume fraction of the fins
ϕ_{cv}	Volume fraction of the cavities
ψ	Area fraction circumscribed by one T-shaped fin

Subscripts

0,1	Index of the branches and stem
cv	Cavity material
c	Cylindrical solid domain
t	Fin material
f	Fluid
max	Maximum

Superscripts

~	Dimensionless

CHAPTER 1

INTRODUCTION

Advanced technologies with the trend of miniaturization requires cooling under extreme heating loads per unit volume [1]. The current literature shows that the heat transfer rate can be enhanced by altering the design of heat generating domain and/or extended surfaces when the temperature difference is constant. The current literature also shows the design corresponding to the maximum heat transfer rate is similar to the designs in the nature. For instance, Cetkin and Oliani [2] showed that the shape of the high-conductivity pathways inserted in a heat generating domain should be similar to the roots of plants. The shapes exist in the nature can be considered as designs with self-assembly feature, however, it should be noted that the current literature also shows these structures were assembled such that the resistance to the flow is minimum. Depending on the objectives of the structures this flow can correspond to the flow of heat, fluid, and/or stress. Adrian Bejan [3-6] stated Constructal Law in order to explain this phenomenon which can be quoted as; "For a finite-size flow system to persist in time (to live), its configuration must change in time such that it provides easier and easier access to its currents (fluid, energy, species, etc.)". The current literature shows the distinct flow configurations (such as river-delta [3], lungs [7], heat generating domain with high-conductivity inserts [8-9] and many more) can be explained or designed in consideration with the constructal law. The literature also includes heat transfer enhancement studies via using constructal fins, cavities and conductive pathways.

Here we include the effect of shape change (fins and cavities) on the fluid flow and heat transfer unlike in the current literature. The alterations in the shape of fins and cavities disturb the velocity field which affects the convective heat transfer coefficient. Therefore, the fluid flow and heat transfer parts of the convection problem were solved simultaneously in order to uncover the effect of shape on both the heat transfer surface area increment and the change in the fluid flow characteristics. Here, we also document the shape of the fins and cavities corresponding to the maximum heat transfer rate in both parallel and cross-flows.

1.1. Fins

Bejan and Almogbel [10] performed a study that geometric optimization of T-shaped fin assemblies with the objective of maximizing global thermal conductance of the assembly under fixed total volume and fin material constraints. Additionally, three types of the fin assembly have been optimized in this study, T-shaped, Tau shaped and Umbrella shaped of cylindrical fins as shown in Fig. 1.1. The study reports that constructal optimization can maximize the global thermal conductance of the assemblies, however the optimization yields different gains for each specific design configuration.

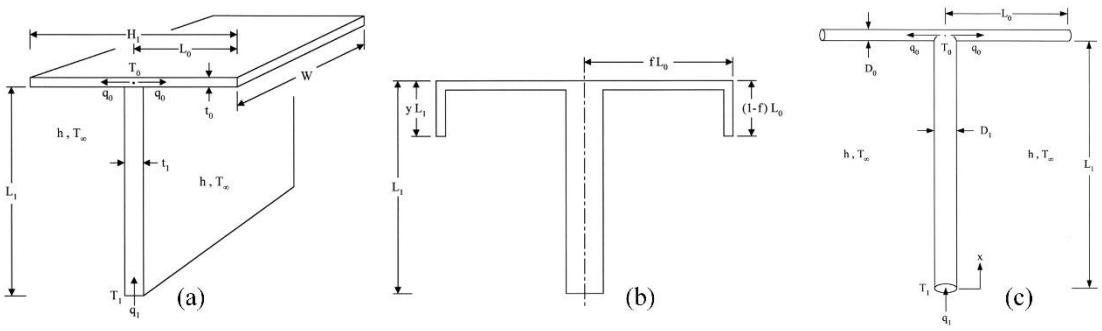

Figure 1.1 Fin assemblies; (a) T-shaped, (b) Tau-shaped, (c) Umbrella shaped [10].

Lorenzini and Moretti [11] documented the numerical simulation results of the study that carried out by Bejan and Almogbel [10] in order to increase the practicality of the results for industrial applications. The results of the study show that the numerical simulation results are in accord with the Constructal theory results. In addition to the Ref. [10], they showed the temperature distribution of the fin assembly, Fig. 1.2. According to the figure peak temperature field exists at the stem and decreases throughout the branches.

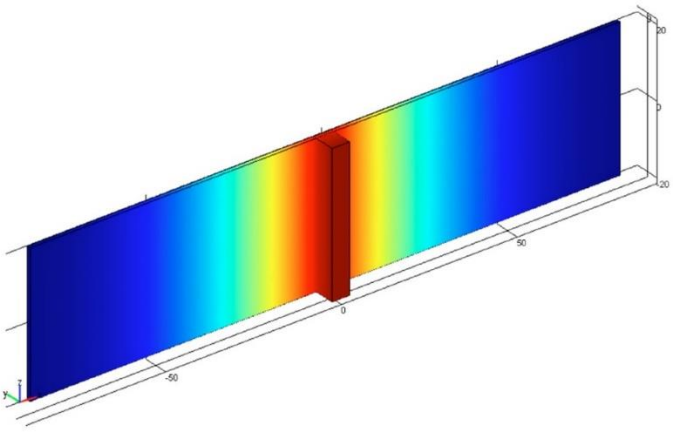

Figure 1.2 Temperature distribution of T-shaped fin assembly [11]

Hazarika et al. [12] showed another approach to optimize the geometry of T-shaped fin. In the study, an analytical method (namely Adomian decomposition method) was used to determine the temperature field, and there are also numerical solution results to validate the current solution. The study includes heat and mass transfer simultaneously. In other words, the constructal T-shaped fin assembly was assumed in fully wet conditions under dehumidifying conditions, and the differences of temperatures and humidity ratios play important role on heat and mass transfer, respectively. According to the results of this study, increase in the length ratio (the ratio of the length of branch and the length of stem) decreases fin efficiency and increases fin effectiveness, while increase in the thickness ratio (the ratio between the thicknesses of branch and stem) enhances the both performance parameters. Finally, according to the results of this study, current model have lower value of fin performance and higher value of actual dimensionless heat transfer rate than Ref. [10].

Lorenzini et al. [13] reported a numerical optimization study which considers T-shaped assembly of fins attached to the cylindrical solid body. There is a uniform heat generation throughout the cylindrical solid body where the material properties and heat transfer coefficient considered as constant. Outer surface of the cylindrical solid body is adiabatic. Therefore, convection takes place only between the steady stream and the surfaces of the fins. The objective of this study is that minimizing maximum excess temperature. In order to minimize the temperature, they investigated the effect of geometric parameters which are thickness ratio (thicknesses of the branch and the stem, (t_1/t_0), length ratio (lengths of the branch and the stem, (L_1/L_0), area fraction of the fins (φ), area that circumscribed by one fin (ψ), and number of fins on the temperature. Some

of the best configurations corresponding to the thermal performance in Ref. [13] can be seen in Fig. 1.3. According to the figure, when the number of fins equals to 2, optimal configuration has slender tributaries and thick stem. However, when the number of fins becomes greater than 2, there is a limitation of architecture in order to prevent coinciding two adjacent fins each other. Therefore, the optimal configuration has slender stem and short tributaries.

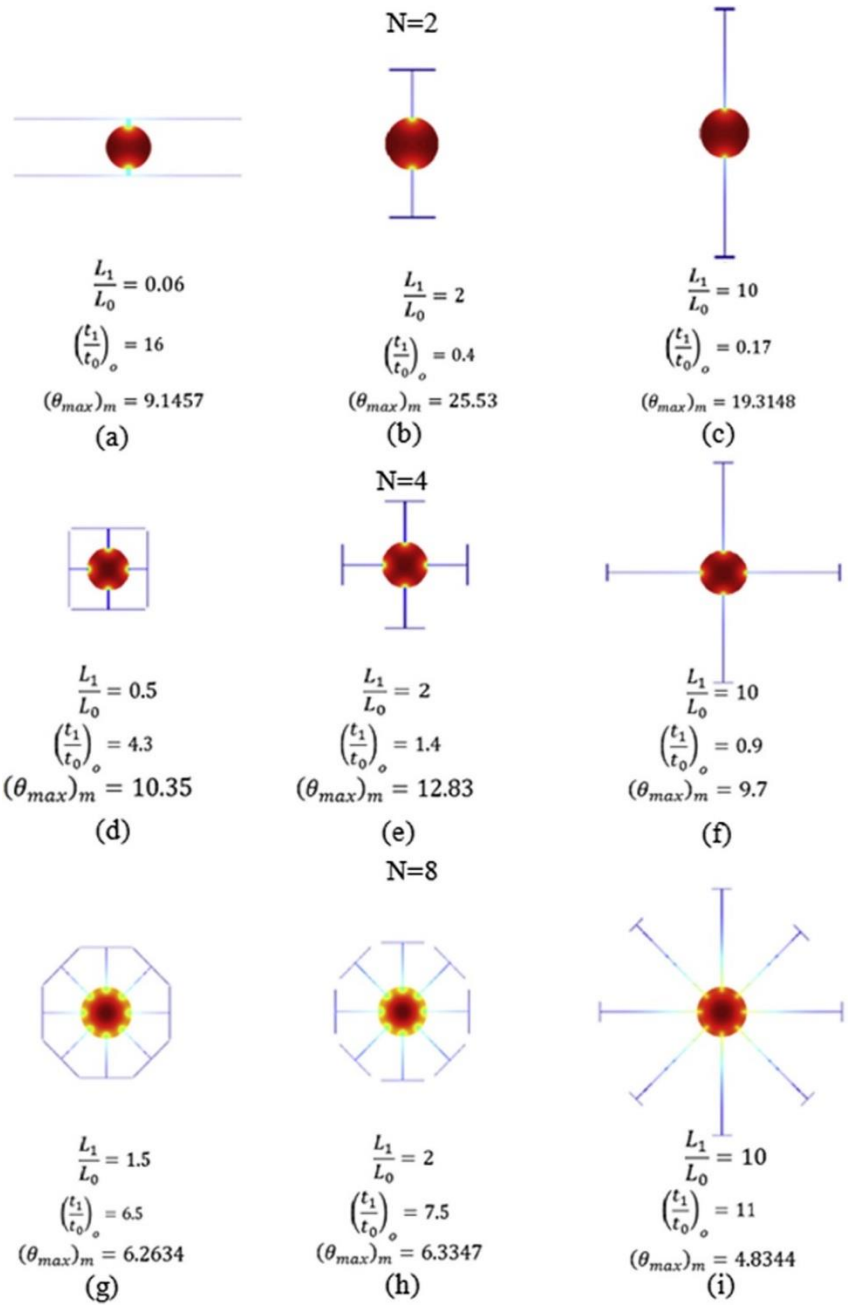

Figure 1.3. Some configurations with high thermal performances [13].

The performance of the various fin shapes have also been studied in the literature. Lorezini et al. [14] performed a geometric optimization of Y-shaped assembly of fin as shown in Fig. 1.4. The objective of the study is that finding the design which corresponds to the minimum thermal resistance subject to the total volume and fin material constraints. For finding the optimal shape, they optimized three parameters; the external shape of the assembly (L_1/L_0), the ratio of plate-fin thicknesses (t_1/t_0) and the angle between the branches and the x-direction (α). The angle becomes an additional degree of freedom to the T-shaped fin of Ref. [10].

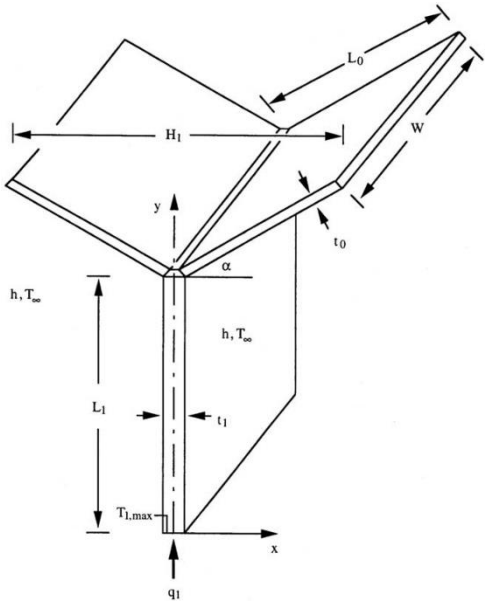

Figure 1.4 Y-shaped assembly of fins [14]

Finally, they concluded that Y-shaped assembly has better thermal performance than the T-shaped fins presented in the literature for the constraints and assumptions they had in their study. Additionally, it was also showed that the optimal Y-shaped fin has larger plate-fin thickness ratio than the T-shaped fin while (L_1/L_0) increases.

Lorenzini and Rocha [15] documented the geometries of T- and Y-shaped fins which corresponds to the minimum thermal resistance with considering the Constructal law. There is a cavity between the branches of the assembly, in addition, the constant convective heat transfer coefficient was assumed along the fins surfaces during the numerical studies. Furthermore, there were three constraints during the optimization as the total volume, the volume of fin material and the volume of the cavity. Reference [15] shows that the global thermal resistance decreases as the height of the cavity which is

penetration to the fin increases. Finally, according to the results, decrease in the length scales of the cavity and increase in the fin material increases thermal performance.

Lorenzini et al. [16] attached two additional surfaces to the T- and Y-shaped assembly of fins and named as complex assembly of fins. The total volume of the two extended surfaces becomes an additional constraint to the constraints of Ref. [15]. Figures 1.5a and 1.5b show temperature distributions of complex assembly of fins of Ref. [16] and the T-Y shaped configurations of Ref. [15], respectively.

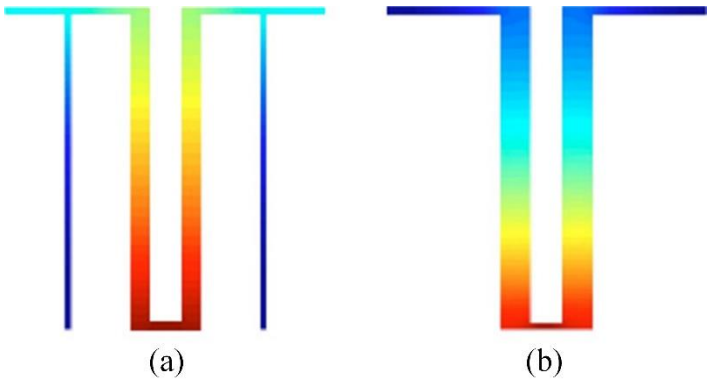

Figure 1.5. Temperature distributions; (a) Complex assembly of fins, (b) T-Y shaped fins of Refs. [15-16].

Figure 1.5 shows that the both complex and T- and Y-shaped designs have a similar temperature distribution. However, the figure shows that the temperature distribution of the complex design near the cavity is more uniform than the T- and Y-shaped design. Whereas, the locations of the peak temperature are alike. Reference [16] also documents the increment in the thermal performance with the design alteration from the T- and Y-shaped to the complex design, which is 32%.

1.2.Cavities

The cavities would also increase the heat transfer surface area similar to the extended surfaces, therefore, they are studied in the literature for heat transfer rate enhancement. The constant heat transfer coefficient assumption is generally used in the studies of the cavities likewise the ones about the fins. A rectangular shaped cavity was optimized with fixed volume by Rocha et al. [17]. The cavity was intruded into the solid conducting trapezoidal wall with internal heat generation and adiabatic outer surfaces. In

addition, they considered three ratios while optimizing the geometry. Figure 1.6 shows the length scales of the cavity, and how the (H_0/L_0) affects the shape of the cavity. The ratios (H_e/H) and (H/L) relate with the external shape of the solid wall and the ratio (H_0/L_0) represents the cavity. According to Rocha et al. [17], the best thermal performance among the all configurations is seen when the aspect ratio equals to 0.1. In other words, minimum overall thermal resistance between the volume and the surroundings exists on the shape with the cavity aspect ratio of 0.1.

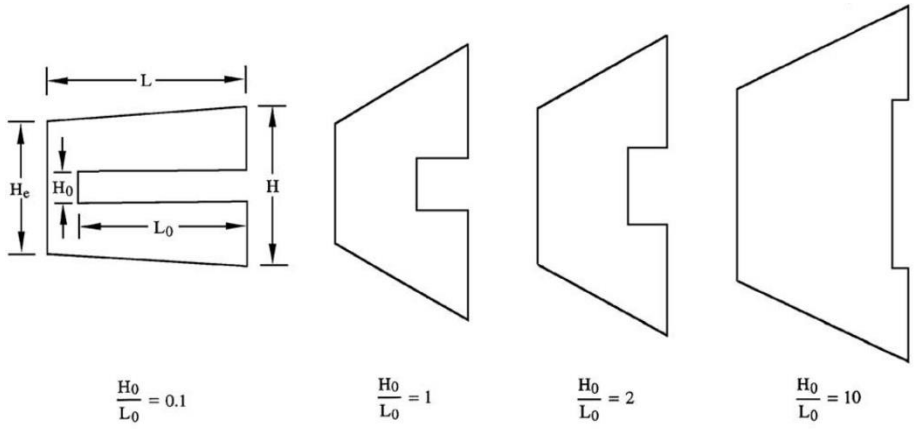

Figure 1.6. The optimal rectangular-shaped cavities [17]

Xie et al. [18] applied constructal theory to optimize a geometry which includes a trapezoidal solid and a T-shaped cavity which intruded into the solid. Figure 1.7 shows the geometry. It can be seen from the figure that the parameters (H_e, H, L) are the dimensions of the trapezoidal solid. The parameters (H_0, L_0) belong to the branches of the cavity, and the parameters (H_1, L_1) represent the size of the stem of the cavity. The outer surfaces are adiabatic and constant material properties with constant heat transfer coefficient assumptions were used. In order to reach to the best thermal performance, they optimized the (H_e/H, H/L, H_1/L_1, H_0/H_1, L_0/L_1) ratios to reach the geometry which reduces maximum excess temperature. They proved that when the ratio (H_e/H) increases the performance also increases, while H_e decreases the optimal stem length of the cavity increases. Furthermore, the most efficient cavity shape has the branches which almost penetrates the solid body.

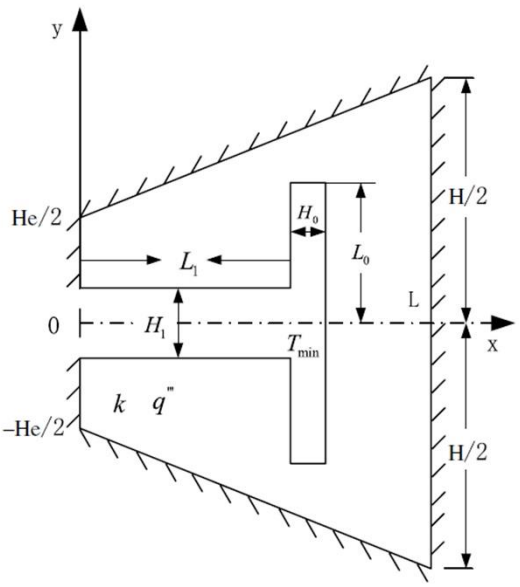

Figure 1.7. T-shaped cavity and the solid conducting wall [18].

Biserni et al. [19] performed a numerical study to optimize two different shapes of cavities that intruded into a solid conducting wall. A rectangular shaped cavity and a T-shaped cavity were considered. Both of the assemblies have the same assumptions which are uniform heat generation and uniform heat fluxes of the outer surfaces of the geometries. The total volume of the geometries and the total volume of the cavities were fixed while the shapes of the cavities can be varied. Finally, they concluded that the T-shaped cavity model has lower thermal resistance than the rectangular shaped one under the same thermal conditions.

Lorenzini et al. [20] studied the use of the convective Y-shaped cavity uncovered with the genetic algorithm in order to minimize the peak temperature of the solid conducting wall, Fig. 1.8. The optimization process was carried out by four degrees of freedom for the several values of the dimensionless heat transfer rate. The first optimized parameter is the aspect ratio of the solid domain (H/L), the second one is the ratio of the lengths of the stem and the branch (L_1/L_0). The third and fourth ones are the ratio of thicknesses of the stem and the branch (t_1/t_0), and the angle between the branch and the x-direction (α). Lorenzini et al. [20] performed the optimization process with two methods; the exhaustive method and the genetic algorithm method. In addition, there is a comparison of the results of these methods. It was observed that the genetic algorithm method requires significantly lower number of simulations than the exhaustive method. In addition, there is not a universal optimal shape for all values of the dimensionless heat

transfer rate. However, increasing of the dimensionless heat transfer rate improves the temperature distribution along the solid domain.

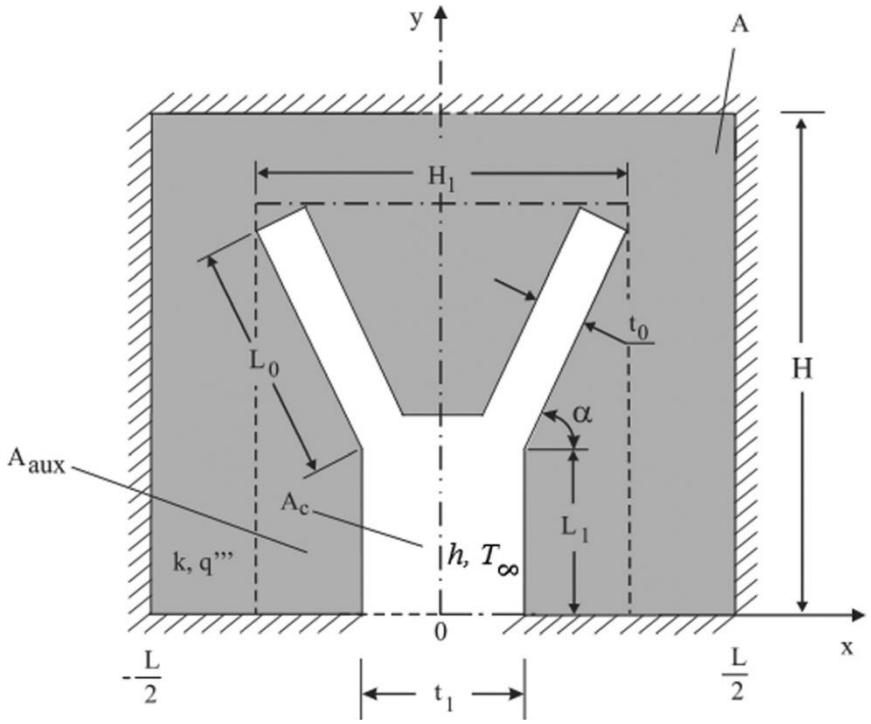

Figure 1.8. Y-shaped cavity and solid conducting wall [20].

Lorenzini and Rocha [21] applied Constructal design to optimize a geometry which includes T-Y shaped cavity and a solid conducting wall. According to the study, likewise the former studies, optimal cavity shape have tendency to almost penetrate the solid body. In addition, the complexity of the geometry can be efficient for improving the thermal performance and Lorenzini and Rocha [21] made a comparison between the rectangular shaped cavity and the T- and Y- shaped one under the same thermal conditions and the area fraction of the cavity corresponding to the thermal performance. They documented that T- and Y- shaped model has greater thermal performance than rectangular shaped one. Figure 1.9 shows the temperature distributions of the optimized geometries for T- and Y- shaped and rectangular shaped cavities. It can be seen that T- and Y- shaped cavity has lower peak temperature and more complex geometry in comparison with the rectangular shaped geometry.

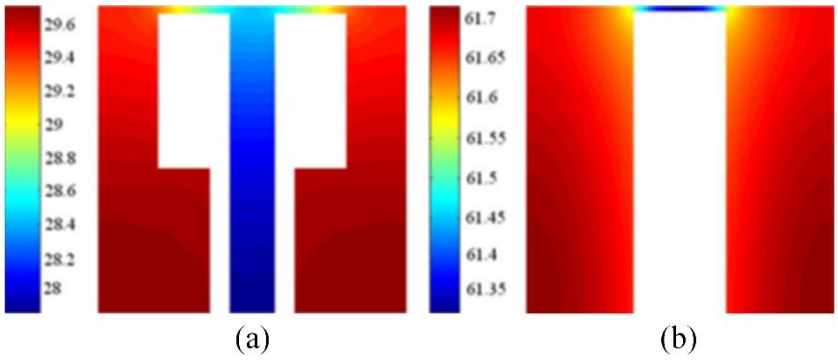

Figure 1.9. Temperature distributions; (a) T-Y shaped cavity, (b) Rectangular-shaped cavity [21]

Lorenzini et al. [22] added two lateral intrusions to the T- and Y- shaped cavity of Ref. [21] for obtaining a complex geometry in order to decrease thermal resistance of the structure. They created two designs according to the positions of the additions as shown in Fig. 1.10.

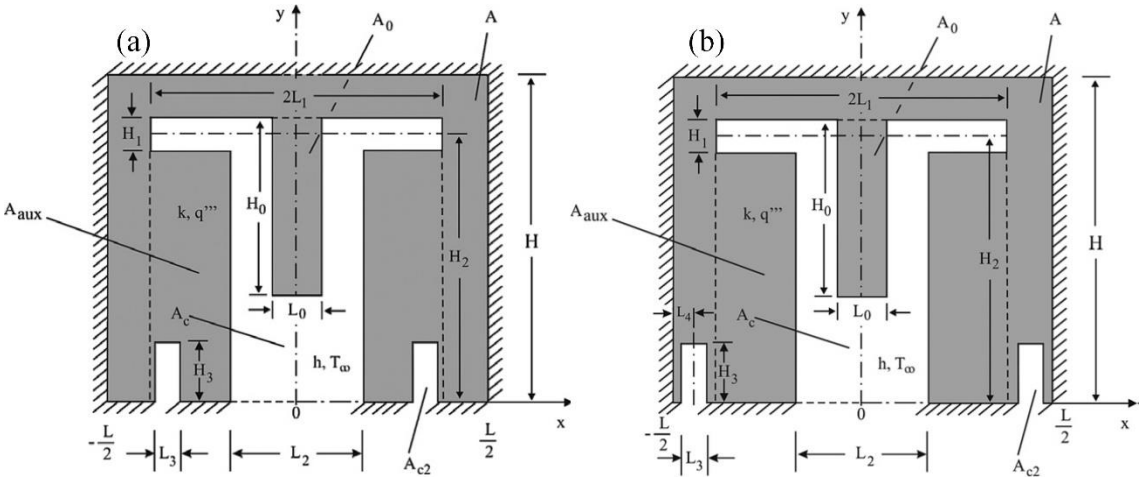

Figure 1.10. T-Y shaped cavity and two additional surfaces; (a) Design 1, (b) Design 2 [22].

According to the Lorenzini et al. [22], Design 2 has better thermal performance than Design 1, because, the intrusions can penetrate longer distance through the solid body in Design 2. In addition, the optimization parameters have different effects on the thermal performance relative to the Design 1 and Design 2. Finally, they showed that Design 2 provides two times better thermal performance than the model of Ref. [21].

Lorenzini et al. [23] showed the optimization process of the rectangular shaped cavities that attached to the heat generating cylindrical solid. The outer surface of the

cylinder is insulated and convective heat transfer only exists between the ambient and the cavity surfaces with constant heat transfer coefficient. The optimization process includes investigations of the effect of the number of cavities, cavity aspect ratio, cavity area fraction and determined dimensionless parameter related with heat transfer coefficient. The results show that, the optimal cavity aspect ratio which minimizes the peak temperature exists. The optimal number of cavities increases while the cavity area fraction and dimensionless heat transfer coefficient increase. In addition, Figure 1.11 illustrates the changes of the temperature distributions corresponding to the number of cavities (N), and the dimensionless parameter (λ) with different cavity aspect ratios and the same cavity area fraction. It can be seen that increment of the dimensionless parameter decreases relatively the area of the hot regions for the same number of cavities. Due to the adiabatic outer surfaces, hot regions are located near the outer surfaces and between two adjacent cavities. In addition, the hot spot is located in the center for several designs due to the varying aspect ratio. Increase in the aspect ratio make the shape of the cavities shorter and thicker. In other words the cavity penetration becomes weak.

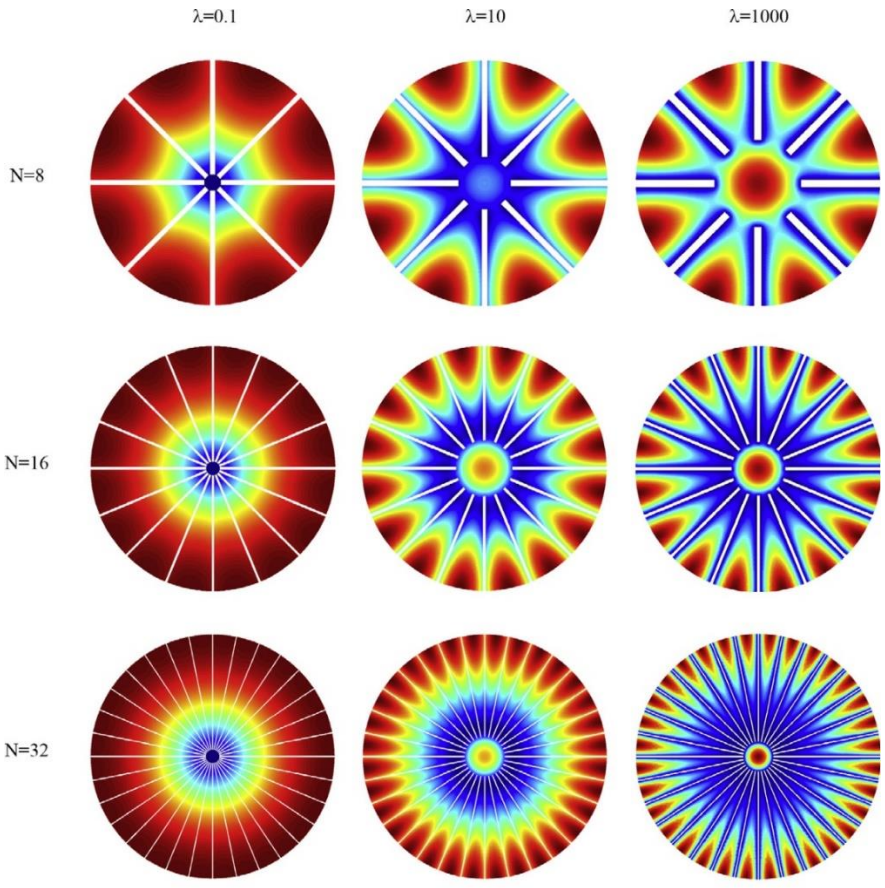

Figure 1.11. Temperature distributions of some optimal shapes [23].

Biserni et al. [24] investigated the effect of using the Constructal H-shaped cavity that intruded into a solid conducting wall corresponding to the thermal performance. The H-shaped cavity includes a stem ($L_2 \times H_2$), two vertical intrusions ($L_1 \times H_1$) and two horizontal rectangles ($2 \times L_0 \times H_0$) as shown in Fig. 1.12. Biserni et al. [24] showed that the H-shaped cavity has four times better thermal performance than the rectangular-shaped cavity and three times better thermal performance than the T-shaped cavity under the same thermal conditions.

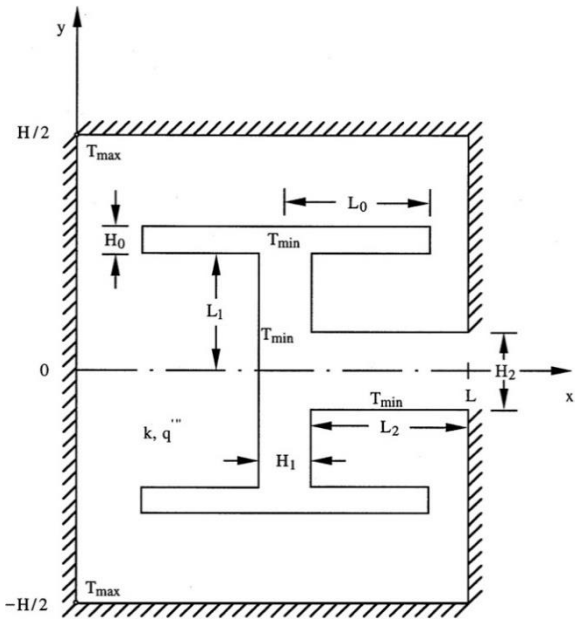

Figure 1.12. H-shaped cavity and the solid conducting domain [24].

1.3 Conductive Pathways

The literature also includes conductive pathways or inverted fins which used to increase the heat transfer rate or decrease the thermal resistance in the systems. Basically, the conductive pathways can be considered as cavities filled with high conductivity materials. Cetkin [1] revealed a study that the maximum temperature of a non-uniformly heated domain can be decreased via using high conductivity inserts embedded to the domain. The tree-shaped inserts have a contact with a heat sink from its stem. The inverted fins increases overall thermal conductivity, so, the peak temperature can be decreased to the desired levels with the less coolant volume. The investigation of the best geometry includes the diameter ratios, lengths of the stem and the branches, the place of the inserts and the number of bifurcation levels. Figure 1.13 illustrates the details of the model.

According to the results, when the boundary layers of the branches almost touch each other, the branches cover greater volume. Therefore, the thermal performance increases.

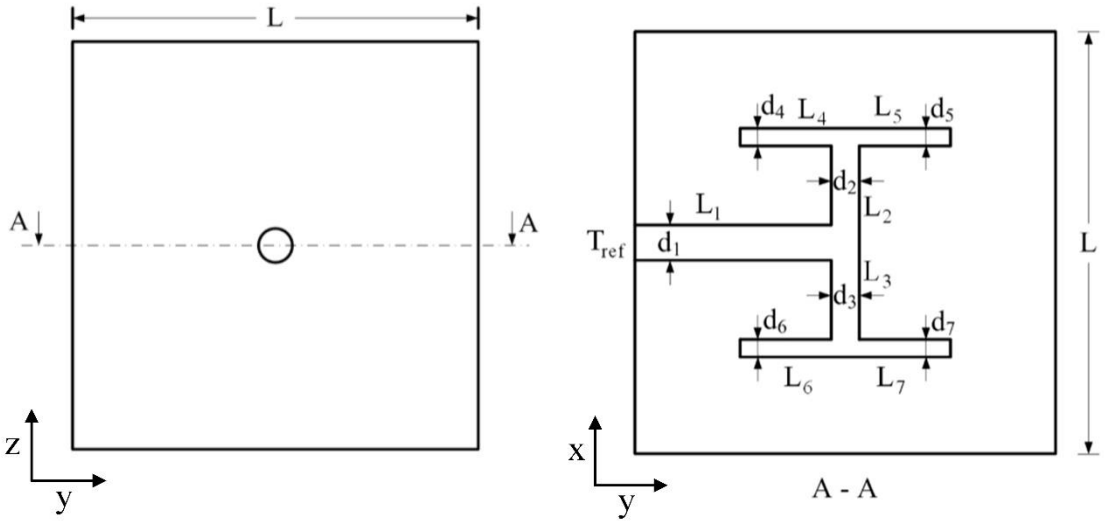

Figure 1.13. High conductivity tree inserted in a cube [1].

Cetkin [25] performed a study to minimize the peak temperature of the heat generating domain by using high conductivity inserts and an embedded channel, as shown in Fig. 1.14. In the study, the place of the high conductivity inserts, Re number and the geometrical ratios which are the aspect ratio of the inserts and the heat generating domain was studied to find the best configuration corresponding to thermal performance. It was suggested that the place of the high conductivity inserts depend on the Re number. For instance, when Re number decreases, the place is advised to be closer to the outlet. In addition, the effects of the volume fraction and the shapes were also documented.

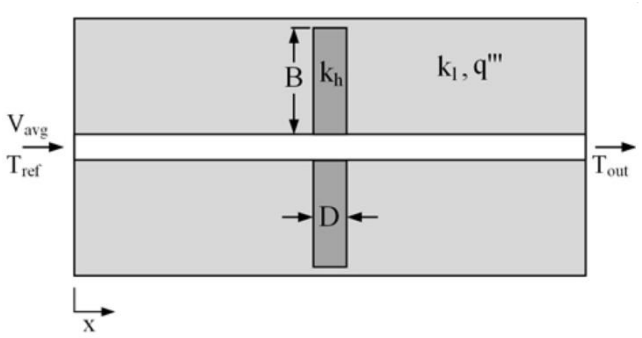

Figure 1.14. Heat generating domain with embedded channel and high conductivity inserts [25].

CHAPTER 2

MODEL AND METHOD

2.1 Cross-Flow

Here, fluid flows in the perpendicular direction to the heat generating cylinder. The numerical model can be two dimensional because the length of the cylinder does not affect the rate of the heat transfer.

2.1.1. T-Shaped Fin

Consider a heat generating cylinder with attached T-shaped fins in a two dimensional unit element, Fig 2.1. The thermal conductivity of the heat generating domain, (q'''), with the size of $\pi \times R^2$is k_c. The thermal conductivity of the T-shaped fins with length scales of (L_1, t_1) and (L_0, t_0) are k_t, and they are placed symmetrically upon the solid body. The area of the fluid domain is fixed, $H_f \times L_f$, and assumed as 50 times greater than the size of heat generating domain while H_f and L_f can vary. The thermal conductivity of the fluid is k_f. The area fraction of T-assembly of fins over cylindrical solid body is $\phi_t = N_t(2L_0t_0 + L_1t_1)/\pi R^2$ where N_t is number of fins, and the area which is restricted by one T-shaped fin is $\psi = 2L_0L_1/\pi R^2$. Two edges of the fluid domain were described as inlet and outlet boundary condition with the size of H_f. Additionally, symmetry boundary condition was implemented on the remaining edges of the fluid domain with the length scale of L_f. Distance in between the tips of fins and the edges that symmetry boundary condition was designated, was kept constant as $2 \times R$.

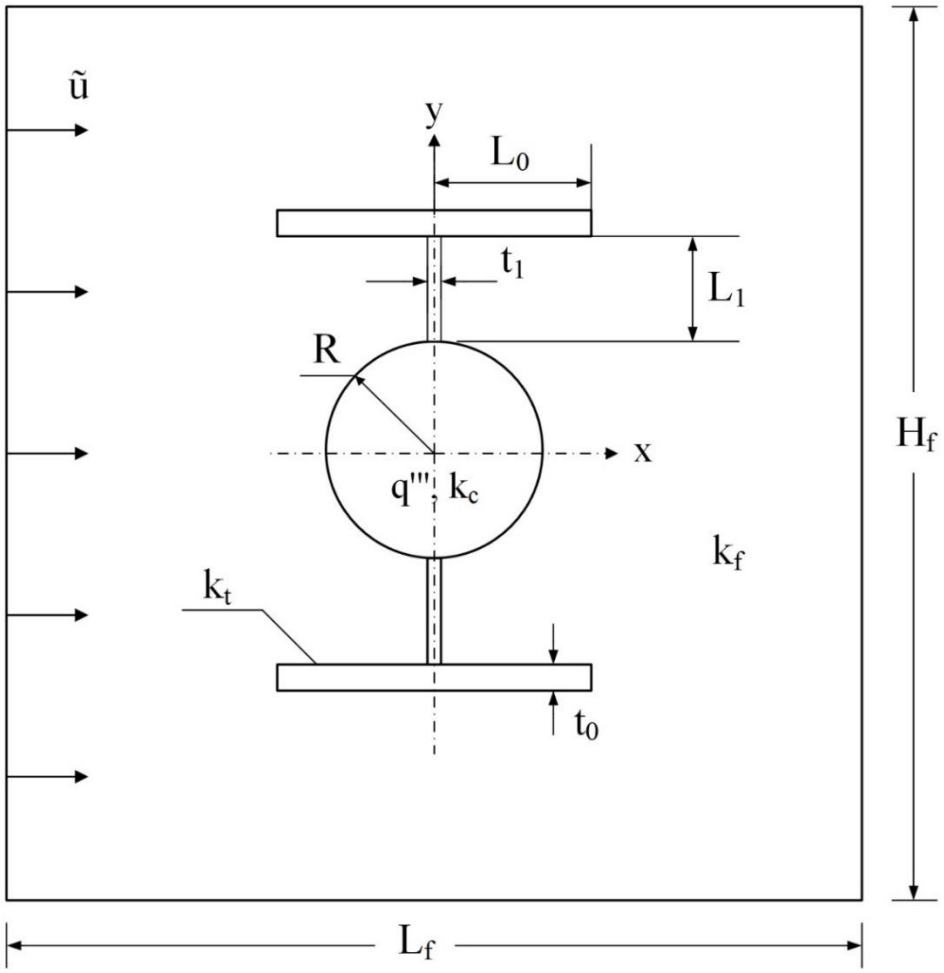

Figure 2.1. Heat generating domain with T-shaped fins in a unit flow domain element.

Throughout the study, Navier-Stokes and Energy equations were solved simultaneously in coupled form. The fluid flow is incompressible and laminar. Heat generation is uniform throughout the heat generating cylindrical domain. Isotropic materials with constant material properties were considered. With these simplifications in mind, Navier-Stokes and Energy equations for the fluid domain become

$$\frac{\partial u}{\partial x}+\frac{\partial v}{\partial y}=0 \tag{2.1}$$

$$u\frac{\partial u}{\partial x}+v\frac{\partial u}{\partial y}=-\frac{1}{\rho}\frac{\partial P}{\partial x}+\nu\left(\frac{\partial^2 u}{\partial x^2}+\frac{\partial^2 u}{\partial y^2}\right) \tag{2.2}$$

$$u\frac{\partial v}{\partial x}+v\frac{\partial v}{\partial y}=-\frac{1}{\rho}\frac{\partial P}{\partial y}+\nu(\frac{\partial^2 v}{\partial x^2}+\frac{\partial^2 v}{\partial y^2}) \tag{2.3}$$

$$\rho c_p\left(u\frac{\partial T}{\partial x}+v\frac{\partial T}{\partial y}\right)=k_f\left(\frac{\partial^2 T}{\partial x^2}+\frac{\partial^2 T}{\partial y^2}\right) \tag{2.4}$$

Here, x and y are spatial coordinates, and u and v are the velocity components corresponding to these coordinates, respectively. In addition, P, ρ, ν, c_p are pressure, density, kinematic viscosity and specific heat at constant pressure of the fluid, respectively.

Energy equations for the heat generating domain and the fins become

$$\frac{\partial^2 T}{\partial x^2}+\frac{\partial^2 T}{\partial y^2}+\frac{q'''}{k_c}=0 \tag{2.5}$$

$$\frac{\partial^2 T}{\partial x^2}+\frac{\partial^2 T}{\partial y^2}=0 \tag{2.6}$$

In order to deduce the dimensionless governing equations, the following non-dimensionalization parameters were selected

$$(\tilde{x},\tilde{y})=\frac{(x,y)}{D} \qquad (\tilde{u},\tilde{v})=\frac{(u,v)D}{\nu} \tag{2.7}$$

$$\tilde{T}=\frac{\left(T-T_{ref}\right)k_f}{q'''D^2} \qquad \tilde{P}=\frac{\left(P-P_{ref}\right)D^2}{\mu\alpha} \tag{2.8}$$

Dimensionless Navier-Stokes and Energy equations become

$$\frac{\partial\tilde{u}}{\partial\tilde{x}}+\frac{\partial\tilde{v}}{\partial\tilde{y}}=0 \tag{2.9}$$

$$\tilde{u}\frac{\partial\tilde{u}}{\partial\tilde{x}}+\tilde{v}\frac{\partial\tilde{u}}{\partial\tilde{y}}=-\frac{1}{Pr}\frac{\partial\tilde{P}}{\partial\tilde{x}}+(\frac{\partial^2\tilde{u}}{\partial\tilde{x}^2}+\frac{\partial^2\tilde{u}}{\partial\tilde{y}^2}) \tag{2.10}$$

$$\tilde{u}\frac{\partial \tilde{v}}{\partial \tilde{x}} + \tilde{v}\frac{\partial \tilde{v}}{\partial \tilde{y}} = -\frac{1}{Pr}\frac{\partial \tilde{P}}{\partial \tilde{y}} + (\frac{\partial^2 \tilde{v}}{\partial \tilde{x}^2} + \frac{\partial^2 \tilde{v}}{\partial \tilde{y}^2}) \tag{2.11}$$

$$\tilde{u}\frac{\partial \tilde{T}}{\partial \tilde{x}} + \tilde{v}\frac{\partial \tilde{T}}{\partial \tilde{y}} = \frac{1}{Pr}(\frac{\partial^2 \tilde{T}}{\partial \tilde{x}^2} + \frac{\partial^2 \tilde{T}}{\partial \tilde{y}^2}) \tag{2.12}$$

$$\frac{\partial^2 \tilde{T}}{\partial \tilde{x}^2} + \frac{\partial^2 \tilde{T}}{\partial \tilde{y}^2} + \frac{k_f}{k_c} = 0 \tag{2.13}$$

$$\frac{\partial^2 \tilde{T}}{\partial \tilde{x}^2} + \frac{\partial^2 \tilde{T}}{\partial \tilde{y}^2} = 0 \tag{2.14}$$

Where Pr is Prandtl number.

The conservation of energy at the interfaces between the cylindrical domain and the T-shaped fins, the fins and the fluid domain, the cylindrical domain and the fluid domain were shown below, respectively.

$$(\frac{\partial \tilde{T}}{\partial \tilde{n}})\Big|_c = \tilde{k}_I(\frac{\partial \tilde{T}}{\partial \tilde{n}})\Big|_t \tag{2.15}$$

$$(\frac{\partial \tilde{T}}{\partial \tilde{n}})\Big|_t = \tilde{k}_{II}(\frac{\partial \tilde{T}}{\partial \tilde{n}})\Big|_f \tag{2.16}$$

$$(\frac{\partial \tilde{T}}{\partial \tilde{n}})\Big|_c = \tilde{k}_{III}(\frac{\partial \tilde{T}}{\partial \tilde{n}})\Big|_f \tag{2.17}$$

Where $\tilde{k}_I = \frac{k_t}{k_c}$, $\tilde{k}_{II} = \frac{k_f}{k_t}$, $\tilde{k}_{III} = \frac{k_f}{k_c}$ and $\tilde{k}_I, \tilde{k}_{II}, \tilde{k}_{III}$ values were chosen as 200, 0.0005, 0.01 respectively.

Dimensionless Navier-Stokes and Energy equations were solved via a finite element software which is Comsol Multiphysics [26]. Table 2.1 shows that the simulation results become independent of mesh size with 197458 number of mesh elements where the criterion is $(\left|{\tilde{T}_{max}}^{n+1} - {\tilde{T}_{max}}^{n}\right|)/{\tilde{T}_{max}}^{n} < 10^{-4}$ was satisfied.

Table 2.1. Mesh dependency test for T-shaped fin model, where $\phi = 0.1, \psi = 0.1$, $L_1/L_0 = 0.01$, $t_1/t_0 = 6, Re = 100, N_t = 2$.

Mesh Number	$\tilde{T}_{max} \times 10^2$	$(\lvert \tilde{T}_{max}{}^{n+1} - \tilde{T}_{max}{}^{n} \rvert)/\tilde{T}_{max}{}^{n}$
2934	2.11357585	$1.4045\ 10^{-1}$
9282	2.41042735	$5.0792\ 10^{-2}$
69450	2.53285729	$8.5639\ 10^{-4}$
119168	2.53502641	$6.0999\ 10^{-4}$
197458	2.53657274	$8.7208\ 10^{-5}$
241470	2.53679395	

Figure 2.2 shows validation of current numerical study relative to Reference [13]. The change of the peak temperature according to different (t_1/t_0) and (L_1/L_0) ratios can be seen in the Fig. 2.2. It shows that there is an optimal ratio (t_1/t_0) which varies with different (L_1/L_0) ratios under assumptions of the constant heat transfer coefficient and adiabatic outer surface of the heat generating cylinder. Figure 2.2 also shows the results of the current study is in accord with the published literature.

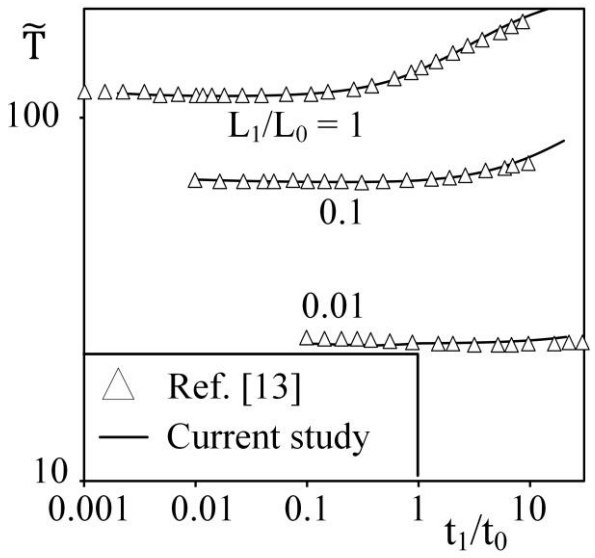

Figure 2.1. Validation of the current study results (T-shaped fins) relative to the results of Ref. [13].

2.1.2 Rectangular-Shaped Cavity

Consider a heat generating domain in which rectangular shaped cavities inserted as shown in Figure 2.3. There are two constraints; total area ($A = \pi \times R^2$) and total cavity area ($A_{cv} = \mathrm{N}_{cv} \times H_{cv} \times L_{cv}$). Where N_{cv} represents the number of cavity.
The area fraction between the total cavity area and the total area is

$$\phi_{cv} = \frac{A_{cv}}{A} \tag{2.18}$$

The fluid domain ($H_f \times L_f$) is 50 times greater than total area of the heat generating solid and the cavities ($\pi \times R^2$) similar to the T-shaped fins of Fig. 2.1. Furthermore, the top and bottom edges of the domain are symmetry boundaries and the distance in between the heat generating domain and the symmetry boundaries is fixed as 3R throughout the analyses.

The conservation of mass and momentum equations for the fluid domain are the same with Eqs. (2.1)-(2.3). The energy equations for the fluid domain and the heat generating domain are the same with Eqs. (2.4) and (2.5), respectively. Similarly, the non-dimensionalization parameters of Eqs. (2.7) and (2.8) were used. Thus, the dimensionless governing equations of Eqs. (2.9) – (2.13) were found. However, due to the absence of the fins the Eq. (2.14) is not included. In addition, the conservation of the energy in between the interface of the fluid and heat generating domain requires Eq. (2.17). Dimensionless cavity area fraction is

$$\phi_{cv} = N_{cv}\widetilde{H}_{cv}\widetilde{L}_{cv} \tag{2.19}$$

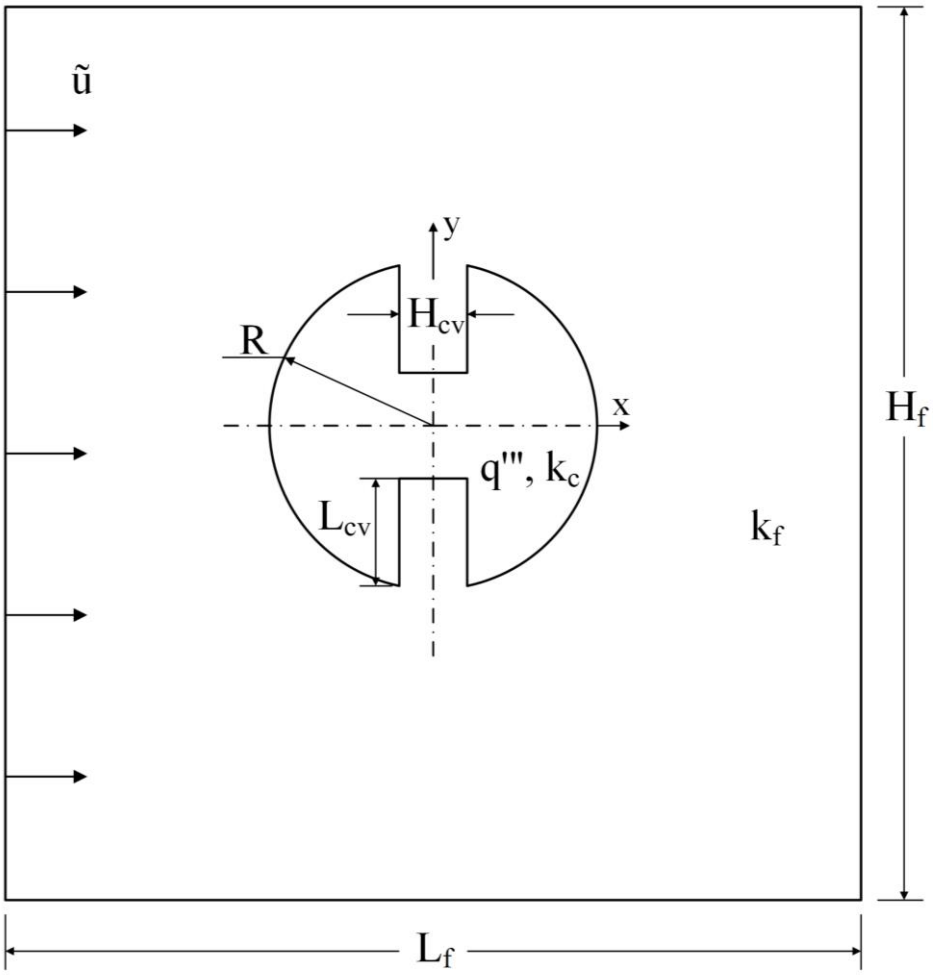

Figure 2.3 Heat generating domain with cavities in a unit fluid domain

Mesh independency test was performed to reach $(\left|\tilde{T}_{max}{}^{n+1} - \tilde{T}_{max}{}^{n}\right|)/\tilde{T}_{max}{}^{n} < 10^{-4}$ criterion and 198516 number of mesh elements was found, as shown in Table 2.2.

Table 2.2. Mesh dependency test for cavity model, where $\phi_{cv} = 0.1, N_{cv} = 4,$ $H_{cv}/L_{cv} = 0.2, Re = 100.$

Mesh Number	$\tilde{T}_{max} \times 10^2$	$(\left\|\tilde{T}_{max}{}^{n+1} - \tilde{T}_{max}{}^{n}\right\|)/\tilde{T}_{max}{}^{n}$
8518	2.2721845	$6.076\ 10^{-3}$
17840	2.28599044	$7.949\ 10^{-3}$
198516	2.30576421	$3.93\ 10^{-5}$
252246	2.30585479	

Figure 2.4 shows the comparison of the current study results with the results of Ref. [23] where the effect of the cavity aspect ratio H_{cv}/L_{cv} on the peak temperature is documented. Figure 2.4 shows the results of the current study agrees with the published results of the Ref. [23].

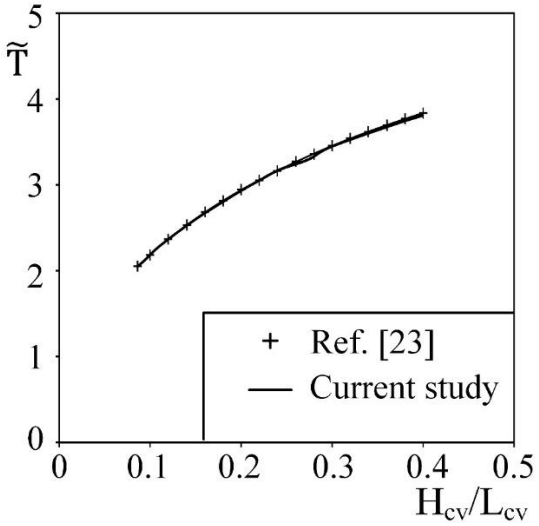

Figure 2.4. Validation of the current study results (cavities) relative to the results of Ref. [23].

2.2 Parallel Flow

In this section fluid flows parallel to the heat generating cylinder It means that fully-wet condition exists for both the fins and the cavities.

2.2.1 T-Shaped Fin

Consider a 3-dimensional heat generating cylinder, $\pi \times R^2 \times W_c$, with four T-shaped fins (L_1, t_1, W_t), (L_0, t_0, W_t), inserted in a fluid domain with the scales of $H_f \times L_f \times W_f$. All lengths about the width of the geometry (W) equals to $(6 \times R)$ for all parallel flow models. Inlet and outlet surfaces are perpendicular to the cylinder's base and top surfaces, the distance in between tip of fins and symmetry planes were kept constant as $R/2$ throughout the analyses for the sake of simplicity. Three-dimensional Navier-Stokes and Energy equations for the fluid domain in steady state are

$$\frac{\partial u}{\partial x}+\frac{\partial v}{\partial y}+\frac{\partial w}{\partial z}=0 \tag{2.20}$$

$$u\frac{\partial u}{\partial x}+v\frac{\partial u}{\partial y}+w\frac{\partial u}{\partial z}=-\frac{1}{\rho}\frac{\partial P}{\partial x}+\nu(\frac{\partial^2 u}{\partial x^2}+\frac{\partial^2 u}{\partial y^2}+\frac{\partial^2 u}{\partial z^2}) \tag{2.21}$$

$$u\frac{\partial v}{\partial x}+v\frac{\partial v}{\partial y}+w\frac{\partial v}{\partial z}=-\frac{1}{\rho}\frac{\partial P}{\partial y}+\nu(\frac{\partial^2 v}{\partial x^2}+\frac{\partial^2 v}{\partial y^2}+\frac{\partial^2 v}{\partial z^2}) \tag{2.22}$$

$$u\frac{\partial w}{\partial x}+v\frac{\partial w}{\partial y}+w\frac{\partial w}{\partial z}=-\frac{1}{\rho}\frac{\partial P}{\partial z}+\nu(\frac{\partial^2 w}{\partial x^2}+\frac{\partial^2 w}{\partial y^2}+\frac{\partial^2 w}{\partial z^2}) \tag{2.23}$$

$$\rho c_p\left(u\frac{\partial T}{\partial x}+v\frac{\partial T}{\partial y}+w\frac{\partial T}{\partial z}\right)=k_f(\frac{\partial^2 T}{\partial x^2}+\frac{\partial^2 T}{\partial y^2}+\frac{\partial^2 T}{\partial z^2}) \tag{2.24}$$

Energy equations for heat generating domain and fins become

$$\frac{\partial^2 T}{\partial x^2}+\frac{\partial^2 T}{\partial y^2}+\frac{\partial^2 T}{\partial z^2}+\frac{\mathrm{q}'''}{k_c}=0 \tag{2.25}$$

$$\frac{\partial^2 T}{\partial x^2}+\frac{\partial^2 T}{\partial y^2}+\frac{\partial^2 T}{\partial z^2}=0 \tag{2.26}$$

Dimensionless parameters for the three dimensional model are

$$(\tilde{x},\tilde{y},\tilde{z})=\frac{(x,y,z)}{D}\qquad(\tilde{u},\tilde{v},\tilde{w})=\frac{(u,v,w)D}{\nu} \tag{2.27}$$

$$\tilde{T}=\frac{\left(T-T_{ref}\right)k_f}{\mathrm{q}'''D^2}\qquad\tilde{P}=\frac{\left(P-P_{ref}\right)D^2}{\mu\alpha} \tag{2.28}$$

Inserting the dimensionless parameters in Eqs. (2.27) and (2.28) yield the dimensionless Navier-Stokes and Energy equations are

$$\frac{\partial \tilde{u}}{\partial \tilde{x}} + \frac{\partial \tilde{v}}{\partial \tilde{y}} + \frac{\partial \tilde{w}}{\partial \tilde{z}} = 0 \tag{2.29}$$

$$\tilde{u}\frac{\partial \tilde{u}}{\partial \tilde{x}} + \tilde{v}\frac{\partial \tilde{u}}{\partial \tilde{y}} + \tilde{w}\frac{\partial \tilde{u}}{\partial \tilde{z}} = -\frac{1}{Pr}\frac{\partial \tilde{P}}{\partial \tilde{x}} + \left(\frac{\partial^2 \tilde{u}}{\partial \tilde{x}^2} + \frac{\partial^2 \tilde{u}}{\partial \tilde{y}^2} + \frac{\partial^2 \tilde{u}}{\partial \tilde{z}^2}\right) \tag{2.30}$$

$$\tilde{u}\frac{\partial \tilde{v}}{\partial \tilde{x}} + \tilde{v}\frac{\partial \tilde{v}}{\partial \tilde{y}} + \tilde{w}\frac{\partial \tilde{v}}{\partial \tilde{z}} = -\frac{1}{Pr}\frac{\partial \tilde{P}}{\partial \tilde{y}} + \left(\frac{\partial^2 \tilde{v}}{\partial \tilde{x}^2} + \frac{\partial^2 \tilde{v}}{\partial \tilde{y}^2} + \frac{\partial^2 \tilde{v}}{\partial \tilde{z}^2}\right) \tag{2.31}$$

$$\tilde{u}\frac{\partial \tilde{w}}{\partial \tilde{x}} + \tilde{v}\frac{\partial \tilde{w}}{\partial \tilde{y}} + \tilde{w}\frac{\partial \tilde{w}}{\partial \tilde{z}} = -\frac{1}{Pr}\frac{\partial \tilde{P}}{\partial \tilde{z}} + \left(\frac{\partial^2 \tilde{w}}{\partial \tilde{x}^2} + \frac{\partial^2 \tilde{w}}{\partial \tilde{y}^2} + \frac{\partial^2 \tilde{w}}{\partial \tilde{z}^2}\right) \tag{2.32}$$

$$\tilde{u}\frac{\partial \tilde{T}}{\partial \tilde{x}} + \tilde{v}\frac{\partial \tilde{T}}{\partial \tilde{y}} + \tilde{w}\frac{\partial \tilde{T}}{\partial \tilde{z}} = \frac{1}{Pr}\left(\frac{\partial^2 \tilde{T}}{\partial \tilde{x}^2} + \frac{\partial^2 \tilde{T}}{\partial \tilde{y}^2} + \frac{\partial^2 \tilde{T}}{\partial \tilde{z}^2}\right) \tag{2.33}$$

$$\frac{\partial^2 \tilde{T}}{\partial \tilde{x}^2} + \frac{\partial^2 \tilde{T}}{\partial \tilde{y}^2} + \frac{\partial^2 \tilde{T}}{\partial \tilde{z}^2} + \frac{k_f}{k_c} = 0 \tag{2.34}$$

$$\frac{\partial^2 \tilde{T}}{\partial \tilde{x}^2} + \frac{\partial^2 \tilde{T}}{\partial \tilde{y}^2} + \frac{\partial^2 \tilde{T}}{\partial \tilde{z}^2} = 0 \tag{2.35}$$

2.2.2 Rectangular-Shaped Cavity

Consider a 3-dimensional cylindrical heat generating domain with the size of $\pi \times R^2 \times W_c$ as shown in Fig. 3.9. Four cavities ($N_{cv} = 4$) were inserted into the heat generating domain with the size of $H_{cv} \times L_{cv} \times W_{cv}$. Fluid enters to a 3-dimensinal unit flow domain and flows along the heat generating cylinder, i.e. parallel flow. The top, bottom, left and right boundaries of the flow domain was specified as symmetry boundaries because the flow domain is a unit domain. The spacing in between the cylinder and symmetry boundaries was also fixed as $(3/2) \times R$. The conservation of mass, momentum and energy equations for the fluid domain is given in Eqs. (2.20)-(2.24). Equation (2.25) documents the energy equation for the heat generating solid domain. After using dimensionless parameters, Eqs. (2.27) and (2.28), on the governing equations,

dimensionless Navier-Stokes and Energy equations for the fluid and the heat generating domain becomes as Eqs. (2.29) – (2.34).

CHAPTER 3

RESULTS

3.1 Cross-Flow

3.1.1 T-Shaped Fin

Figure 3.1 denotes how the geometrical parameters affect the peak temperature with inserted T-shaped fins. The change of the peak temperature according to different values of the parameter ψ can be seen in the Fig. 3.1a. The shape of fins becomes thinner and longer while the parameter ψ increases. Figure 3.1a shows that slender and long fins have better thermal performance. Fig. 3.1b shows that there is an optimal (t_1/t_0) ratio which corresponds to the minimum peak temperature when $\psi = 1$. The optimal ratio increases as (L_1/L_0) ratio decreases from 2 to 0.02. Another parameter that affects the peak temperature is the number of fins, N_t. Figure 3.1c shows the effect of different (L_1/L_0) ratios on thermal performance when N_t equals to 2, 4 and 8. The thermal resistance is smallest when N_t equals to 8. While (L_1/L_0) ratio increases up to 2, the 4 fins corresponds to lower thermal performance than 2 fins configuration. However, as this ratio increases from 2 to 5, 2 fins model shows better thermal performance than the 4 fins configuration.

Temperature distributions and velocity streamlines of the configurations with 2, 4 and 8 number of fins, taken from Fig. 3.1c, are shown in Figs. 3.2, 3.3 and 3.4, respectively.

Figures 3.2a and 3.2b show the temperature distribution and the streamlines of 2 fins configurations when $L_1/L_0 = 0.2$ and $t_1/t_0 = 9$ and $L_1/L_0 = 5$ and $t_1/t_0 = 8$, respectively. Figure 3.2 shows that increasing the stem length of the fin creates a bigger circulation area behind the cylinder. In addition, the increase in the tributary length of the fin, increases the stagnation region in front of the heat generating region. Thus, the temperature of the contact surface of the solid domain with the fluid in Fig. 3.2a has greater temperature than in Fig. 3.2b. Figures 3.2a and 3.2b show that increasing the

length of the stem and decreasing the length of the tributaries decreases the peak temperature. (While L_1/L_0 than 0.1).

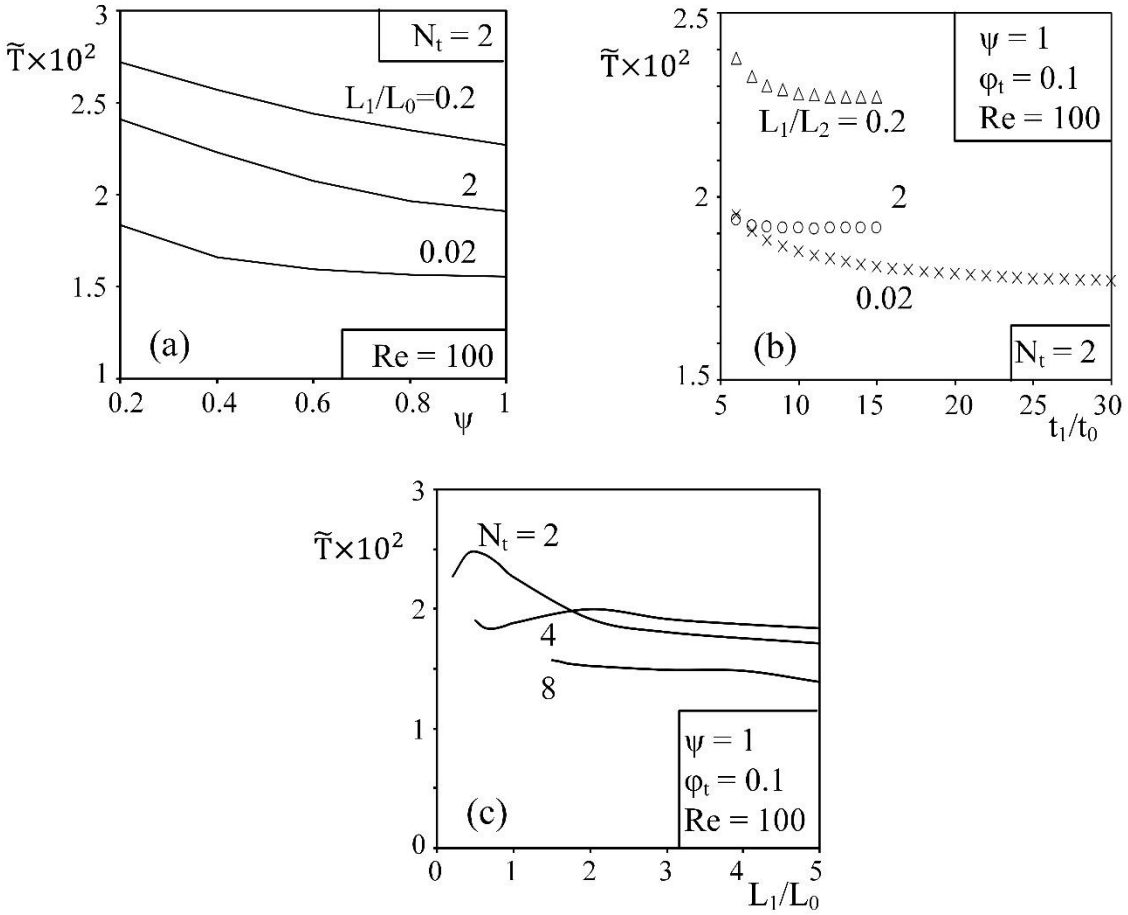

Figure 3.1. The maximum excess temperature of 2-D heat generating domain with fins in cross-flow relative to (a) parameter $'\psi'$, (b) L_1/L_0 and t_1/t_0, (c) L_1/L_0 and number of fins (N_t).

Figure 3.3 shows the temperature distribution and velocity streamline of the 4 fins configurations with $L_1/L_0 = 0.5$ and $t_1/t_0 = 5$ and $L_1/L_0 = 5$ and $t_1/t_0 = 4$. In Figure 3.3a, the tributaries length is so long that it forms almost a closed square, the fluid can not reach the heat generating cylinder and the stems easily. Therefore, the deficiency of circulation weakens convective heat transfer around the cylinder and the stems. In addition, Fig. 3.3 shows that the fluid in between the two adjacent fins yields open cavity type flow which can be seen from the streamlines. Furthermore, Figure 3.3 shows that the convective heat transfer becomes more pronounced due to the cavity flow in between the adjacent stems as the L_1/L_0 ratio increases. Therefore, even the tributary surface area is greater in Fig. 3.3a, the peak temperature is smaller in Fig. 3.3b.

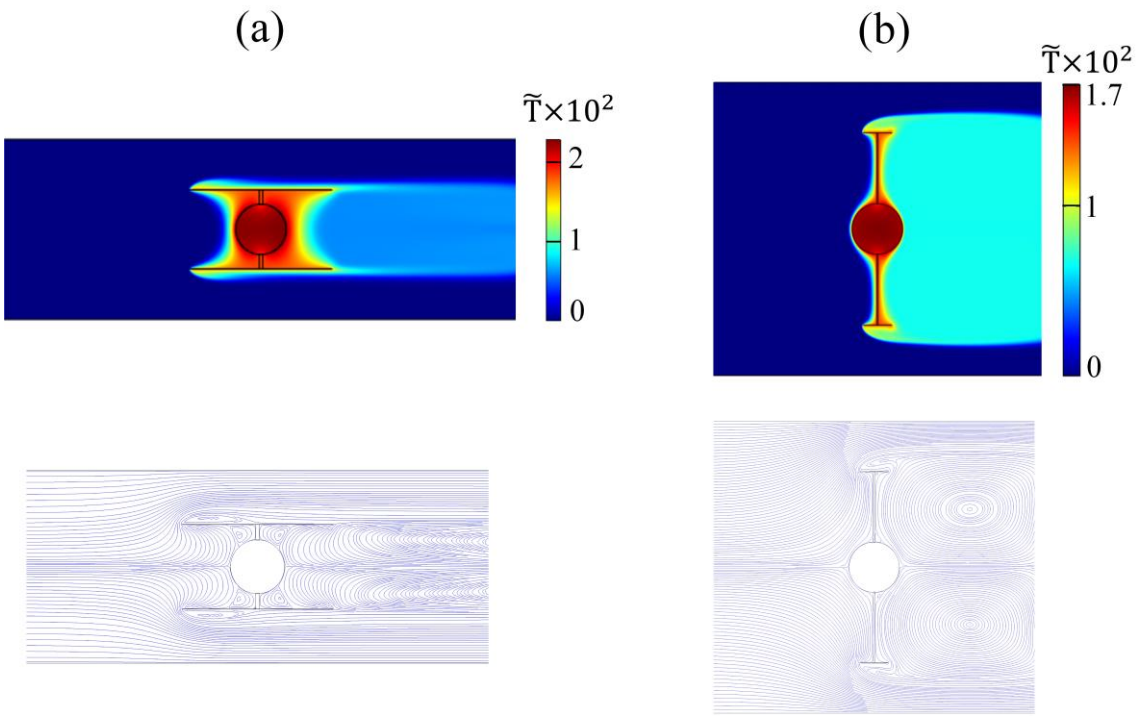

Figure 3.2. Temperature distribution and velocity streamlines when 2 fins attached to the heat generating domain; (a) $L_1/L_0 =$. , $t_1/t_0 =$, (b) $L_1/L_0 = 5$, $t_1/t_0 =$.

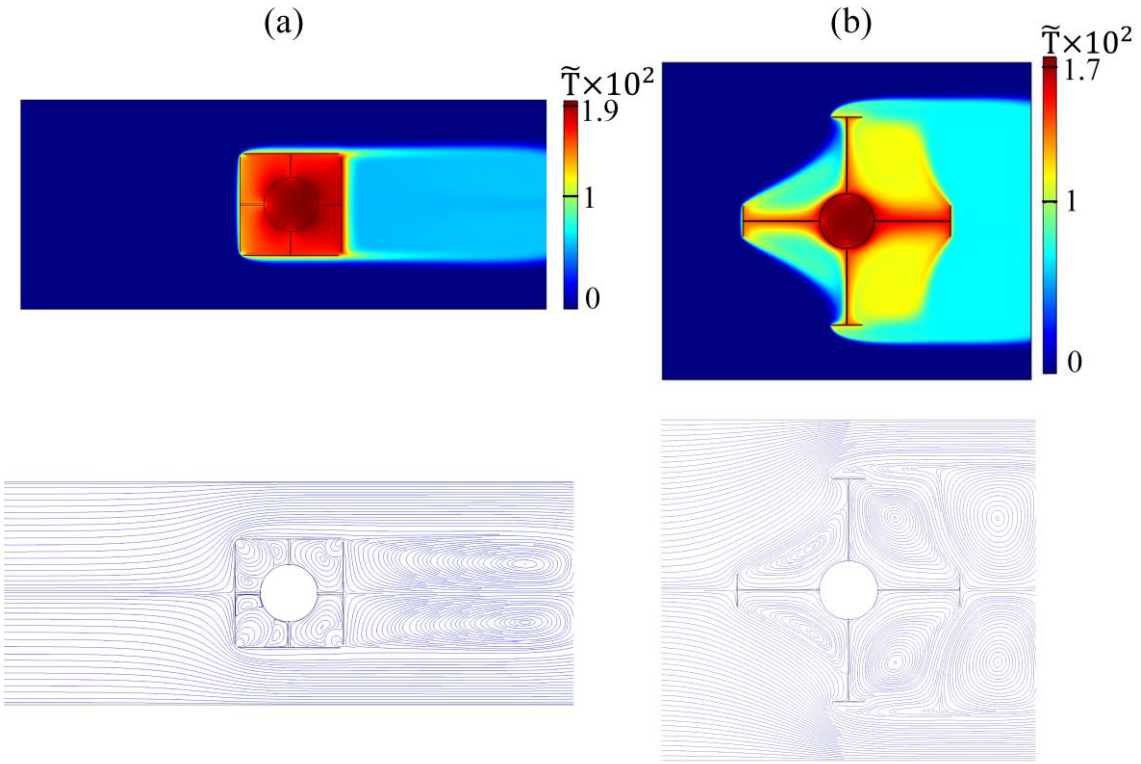

Figure 3.3. Temperature distribution and velocity streamlines when 4 fins attached to the heat generating domain; (a) $L_1/L_0 = 0.5$, $t_1/t_0 = 5$, (b) $L_1/L_0 = 5$, $t_1/t_0 = 4$.

Figure 3.4 shows the temperature distributions and velocity streamlines of two configurations of 8 fins. Convective heat transfer between the stems and the fluid decreases when the circulation of the fluid flow becomes deficient. The best thermal performance is obtained with 8 fins configurations (in comparison to 2 and 4 fins configurations). Figure 3.4 also shows that the vorticities become more homogenous with 8 fins in comparison to the configurations with 4 fins of Fig. 3.3 with the same L_1/L_0 ratio. In addition, the spots which corresponds to the peak temperature are located at the right hand-side of the heat generating cylinder due to the cross-flow.

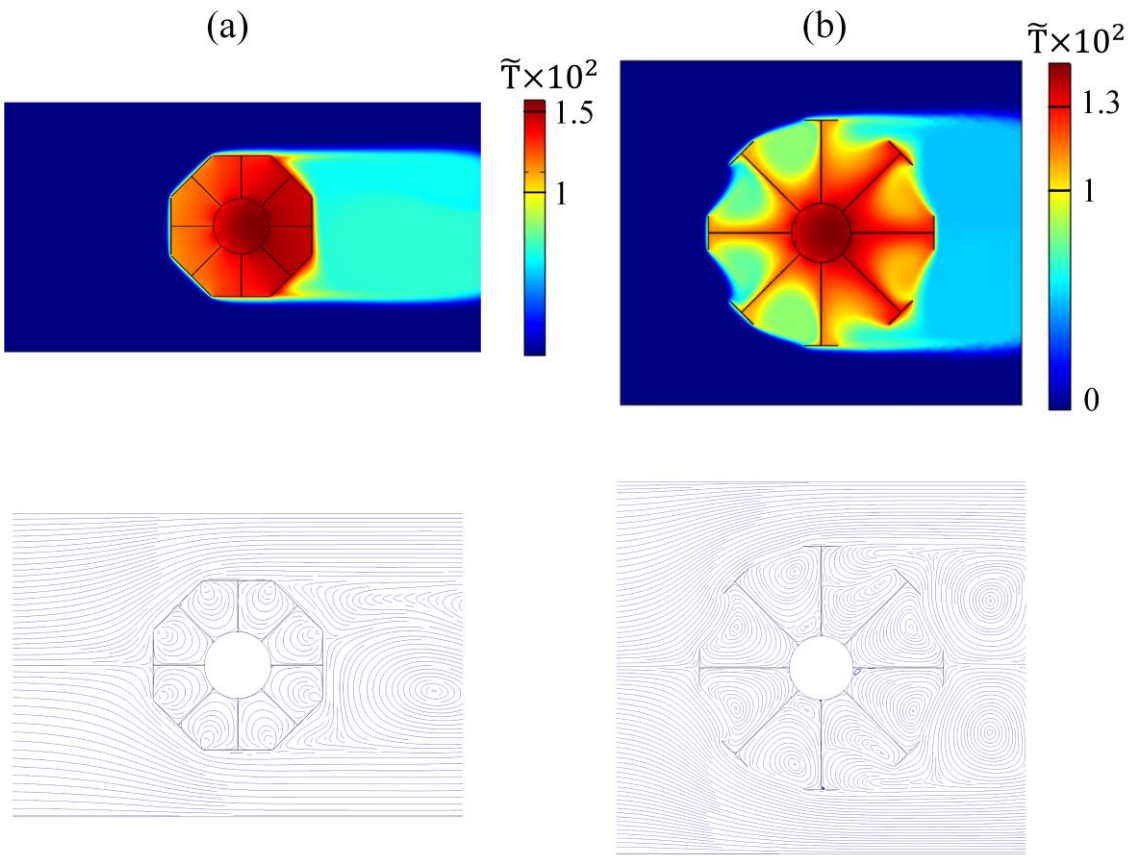

Figure 3.4. Temperature distributions and velocity streamlines when 8 fins attached to the heat generating domain; (a) $L_1/L_0 = 1.5$, $t_1/t_0 = 3$, (b) $L_1/L_0 = 5$, $t_1/t_0 = 3$.

3.1.2 Rectangular-Shaped Cavity

Figure 3.5 shows that there is an optimum aspect ratio (H_{cv}/L_{cv}) which minimizes maximum excess temperature, when N_{cv} equals to 2, 4 and 8. It can be seen from the Figure 3.5 that the optimal aspect ratio decreases as the number of cavities increases. Lower H_{cv}/L_{cv} ratio corresponds to thinner and longer cavity shape while the number of the cavities and ϕ_{cv} are fixed. For the same H_{cv}/L_{cv}, the shape of a cavity becomes thinner and shorter as N_{cv} increases. The cavity shape corresponds to the minimum peak temperature becomes thinner as N_{cv} increases. Therefore, optimal cavity shape in the 8 cavities configuration is the thinnest one among the others as shown in Fig. 3.5.

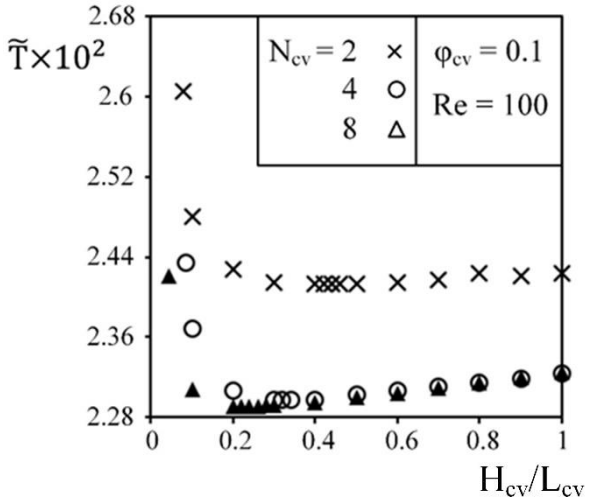

Figure 3.5. The effect of the H_{cv}/L_{cv} ratio on the thermal performance for various number of cavities.

Temperature distributions and velocity streamlines of the configurations that specified in Figure 3.5 are given in Fig. 3.6. Figure 3.6 shows that both the peak temperature and the domain occupied by the peak temperature decreases as N_{cv} increases. In addition, the decrease in the peak temperature diminishes as the number of cavities increases. For instance, the peak temperature decreases 5% and 0.3% as N_{cv} increases from 2 to 4 and from 4 to 8. Velocity streamlines of Fig. 3.6 show that the fluid in the cavities flows with different characteristics depending on their position. However, flow in the most of the cavities can be specified as open cavity flow type. Only exception is the cases where the flow and the cavity are positioned along the same direction. In these cases, the streamlines also show that the fluid enters to the cavity from its center and exits

from its edge. Therefore, the results also show that the position of the cavity is another parameter which affects the convective thermal resistance.

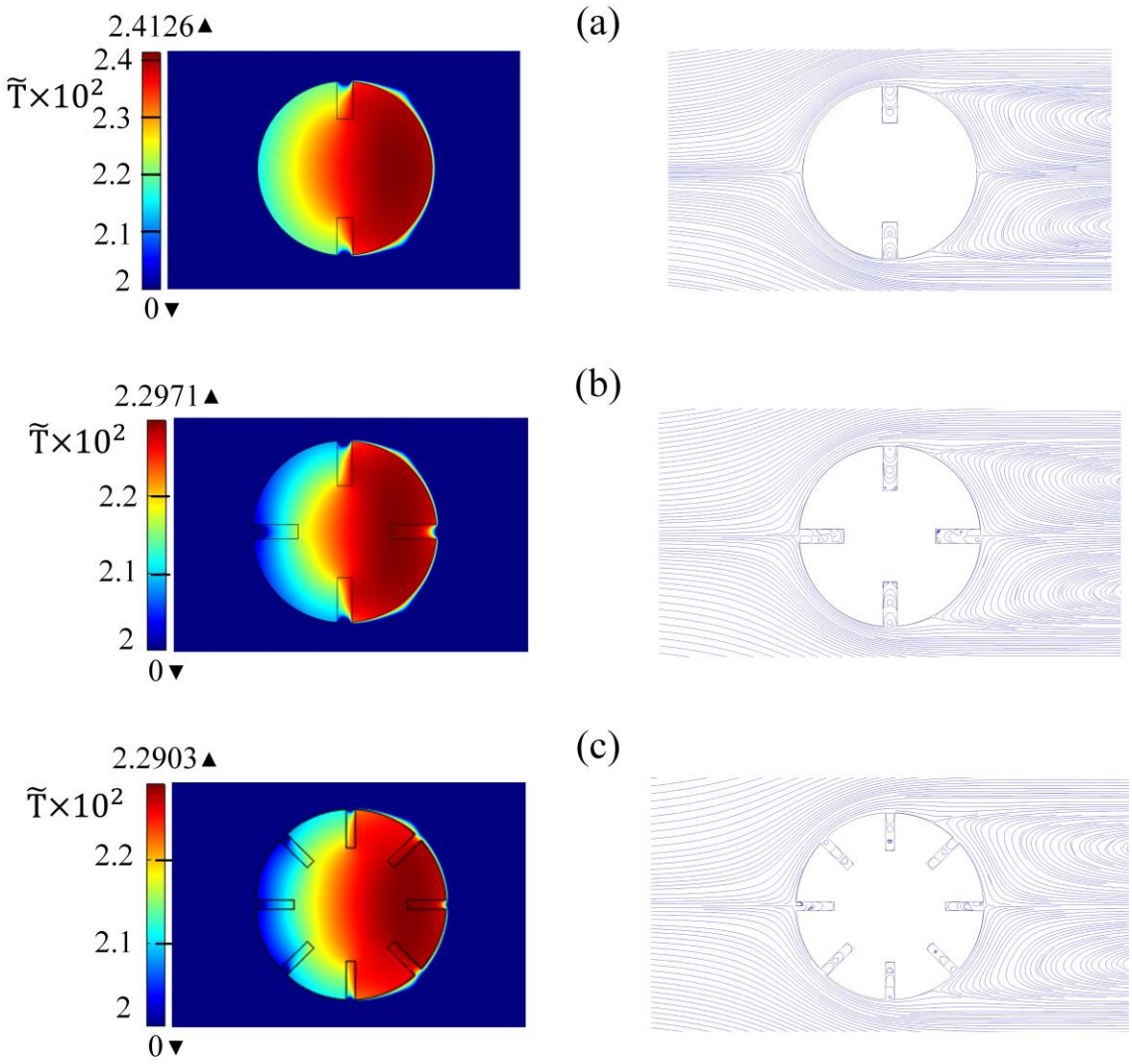

Figure 3.6. Temperature distribution and velocity streamlines for the best performing designs in the Fig. 3.5. ; (a) $H_{cv}/L_{cv} = 0.42$, (b) $H_{cv}/L_{cv} = 0.32$, (c) $H_{cv}/L_{cv} = 0.24$.

The results of both T-shaped fins and cavities show that the overall thermal resistance can be minimized by uncovering the best performing designs. The best performing design exists due to the two conflicting behavior of the area on the heat transfer rate. Heat transfer rate would be expected to increase as the surface area increases. However, this increment also increases resistance to the fluid flow which yields to a decrease in the convective heat transfer coefficient. Therefore, the design corresponding to the minimum peak temperature exists as summarized in Fig. 3.7. Figure 3.7 documents the peak temperature

relative to the Reynolds number for heat generating circular cylinders with only cavities, only T-shaped fins and without cavities and fins. The peak temperature is the greatest for the cylinder without fins and cavities and the smallest for the cylinder with fins. However, Figure 3.7 also shows that the difference in the peak temperature is the greatest with low Re number, and it decreases as the Re increases. For instance, the peak temperature 60.08% greater and 21.57% greater for Re number 10 and 400, respectively.

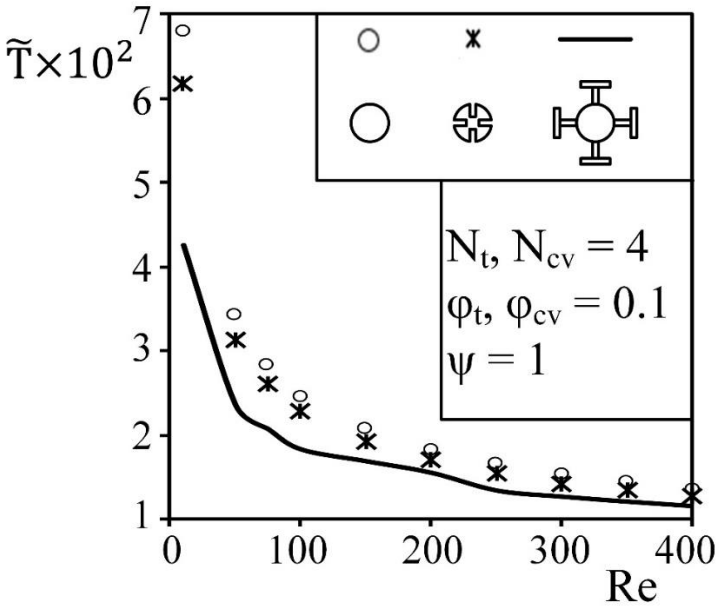

Figure 3.7. The effect of Re number on the peak temperature for the configurations with fins, cavities and no fin and cavity.

3.2 Parallel Flow

3.2.1 T-shaped Fin

Figure 3.8 shows the effect of different parameters on the peak temperature. For instance, Figure 3.8a shows the effect of ψ on the thermal performance for two different L_1/L_0 ratios. The fins become slender (i.e., long and thin) as ψ increases. Schematic drawing of the heat generating cylinder with attached fins can be seen in Fig. 3.8c. Unlike the cross flow configurations, fluid is flowing along the cylinder, therefore, all the surfaces of the cylinder and fins are wetted. In addition, Figure 3.8a shows that decreasing ψ decreases the peak temperature. Therefore, slender tributaries with thick stem corresponds to the smallest resistance for the heat flow. In addition, Figure 3.8a shows

that the effect of ψ becomes more pronounced as the L_1/L_0 ratio increases. However, the peak temperature is minimum with the smallest L_1/L_0 ratio and ψ. Here, the smallest L_1/L_0 ratio was selected as 0.5 in order to eliminate the branches to overlap.

Figure 3.8b shows the effect of t_1/t_0 on the peak temperature for various L_1/L_0 ratios when ψ is 1. Increasing the t_1/t_0 ratio decreases the peak temperature for all L_1/L_0 ratios. However, increasing the t_1/t_0 ratio from 1 to 5 yields a steep decrease then the effect of t_1/t_0 ratio on the peak temperature begins to diminish. In addition, this diminishing is more pronounced as L_1/L_0 ratio increases. Furthermore, Figure 3.8b also shows that the peak temperature decreases and t_1/t_0 ratio increases.

Figure 3.8c documents the effect of L_1/L_0 ratio on the peak temperature with the optimized t_1/t_0 ratios of Fig. 3.8b. Figure 3.8c explicitly shows that increasing the L_1/L_0 ratio increases the peak temperature which is inferred in Figure 3.8b. In addition, Figure 3.8c also shows that the relation between the L_1/L_0 ratio and the peak temperature is power law with less than 1. Overall, Figure 3.8 documents that decreasing ψ and L_1/L_0 ratio and increasing t_1/t_0 ratio decrease the peak temperature in the heat generating cylinder.

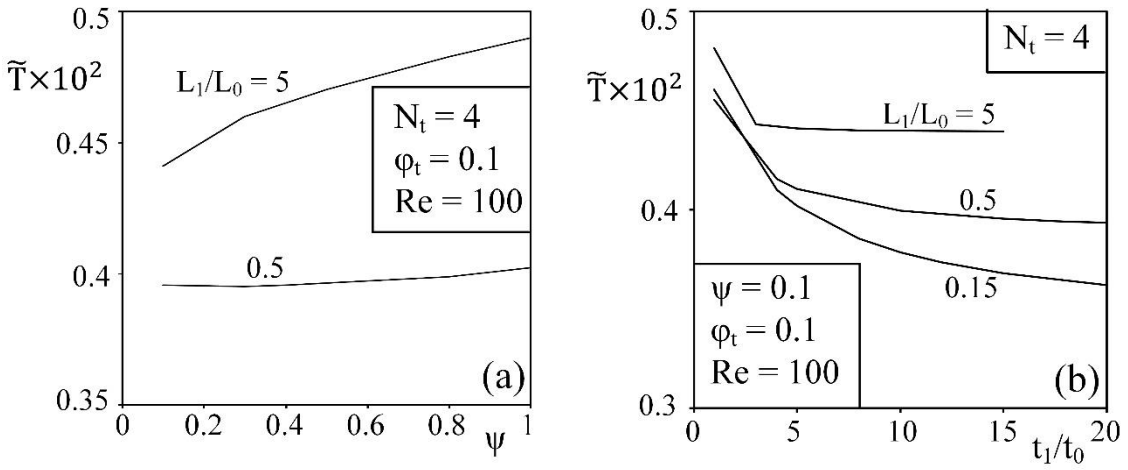

Figure 3.8. The maximum excess temperature of 3-D heat generating domain with fins in parallel flow relative to (a) ψ, (b) t_1/t_0, (c) L_1/L_0.

(cont. on next page)

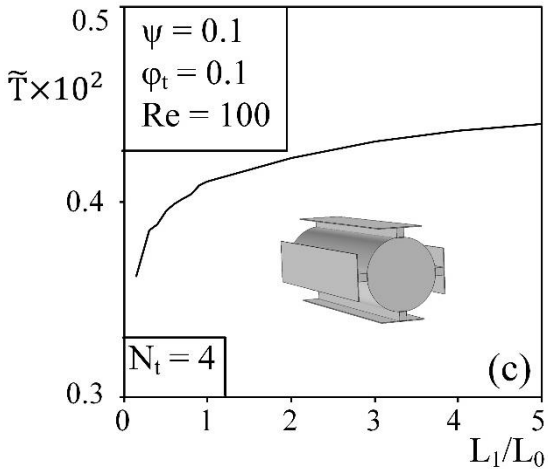

Figure 3.8. (Cont.)

3.2.2 Rectangular-Shaped Cavity

Figure 3.9 shows how the length scales of the cavity affect the peak temperature in the heat generating domain where the volume of the cavities is fixed. Figure 3.9 shows that thinner and longer cavity shapes (i.e., low H_{cv}/L_{cv} ratios) corresponds to low peak temperature values. Increasing the H_{cv}/L_{cv} ratio increases the peak temperature. However, increasing H_{cv}/L_{cv} from 0.1 to 1 increases the peak temperature around 4%. Figure 3.9 also shows that in parallel flow case the cavities begins almost near the origin of the cylinder provides the smallest peak temperature. Therefore unlike in the cross-flow case, the convective heat transfer coefficient is almost uniform and the shape optimization yields to decrease in the conductive resistances in between the cavity surface and the heat generating domain. Therefore, the results of Figure 3.9 is in accord with the results of Ref. [23] where the convective heat transfer coefficient was specified for the cavity surfaces. In addition, unlike in the cross-flow cases, the peak temperature occurs in the middle of the cylinder because the cooling outside of the cylinder is uniform throughout the heat generating surface.

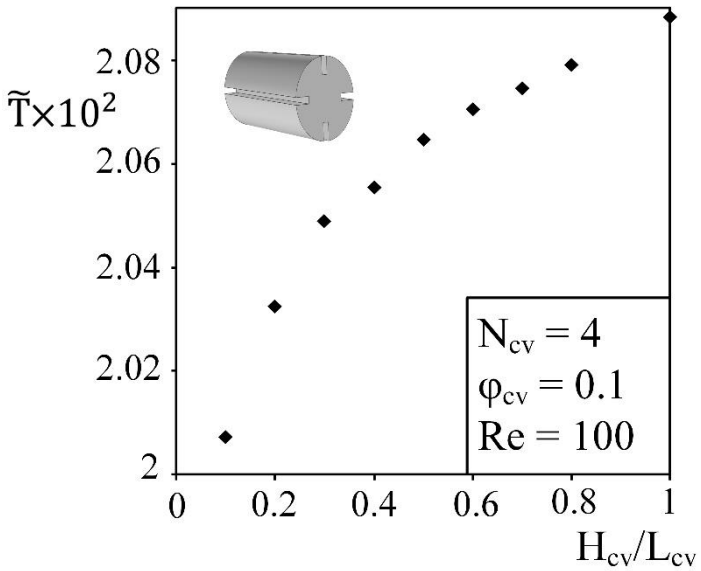

Figure 3.9. The effect of H_{cv}/L_{cv} on the peak temperature.

CHAPTER 4

CONCLUSION

This study shows that the peak temperature of a uniformly heated cylinder can be minimized via using the rectangular shaped cavity or the T-shaped fin and also changing the shapes of the both. In addition, this study also shows there is a design (for both cavity and fin) which provides the minimum thermal resistance for a set of constraints and assumptions. It was expected that the changes in the flow type would also alter the best performing design. Therefore, the cross and parallel flow cases were simulated for both cavities and fins. Furthermore, the effect of the fluid flow on the heat transfer were uncovered by solving the energy equation simultaneously with the Navier-Stokes equations.

For the fin model with the cross-flow, total fin area fraction and the area of the heat generating cylinder was fixed. In order to document the best performing geometry, the effect of the ψ, and the geometric ratios which L_1/L_0 and t_1/t_0 were investigated for various number of fins. According to the results, the design with $L_1/L_0 = 5$ and $t_1/t_0 = 3$ and $N_t = 8$ which corresponds to the best thermal performance. In addition, the thermal performance becomes the worst with $L_1/L_0 = 0.4$ and $t_1/t_0 = 4$ and $N_t = 2$. Thus, the peak temperature of the best configuration has 43.75% lower peak temperature than the worst one.

For the cavity model with cross-flow, the total cavity area and the total area (the heat generating domain and the cavity) are fixed. In addition, the cavity area fraction and the heat generation rate are in accord with the study of the cross-flow fin models with the the fin area fraction and the heat generation rate. In order to decrease the thermal resistance, we investigated the effect of the cavity aspect ratio H_{cv}/L_{cv} for different cavity numbers (N_{cv}). According to the results, the peak temperature can be decreased with the change of the cavity aspect ratio H_{cv}/L_{cv} nearly 7.4% for the two cavities, 5.64% for the four cavities and 5.42% for the 8 cavities. As it can be seen, when the number of the cavity increases the effect of the aspect ratio decreases. However, the best configuration of the 8 cavities has nearly 5% lower peak temperature than the best of the 2 cavities.

For the cross-flow configurations, we found that the best shape of the fins has 39.47% greater thermal performance than the best of the cavity under the same thermal conditions. In addition, the effect of the Re number on the thermal performance of the fins and the cavities was also documented. For instance, when Re number equals 10 and 400 for the best model of the 4 fins, the peak temperature is 60.08% and 21.57% smaller than the peak temperature for the no fin and no cavity model, respectively.

For the fin configurations while the total fin volume and the volume of the cylinder are fixed, the effect of the ψ is not the same with the cross-flow case. It means that rather than long and thin shapes, the thick and short stem with slender tributaries have better thermal performance. According to the results for various t_1/t_0 and L_1/L_0, the peak temperature difference between the best and the worst optimized fin shapes become nearly 17.76%.

For the cavity model with parallel flow case, in order to decrease thermal resistance, the cavity aspect ratio was investigated with the fixed total cavity volume and the total volume. The results show that thin and long cavity shapes decrease the thermal resistance. For instance, when $H_{cv}/L_{cv} = 0.1$, the peak temperature is 3.86% smaller than the one with $H_{cv}/L_{cv} = 1$.

Last, the best configuration of the fin model has nearly 82% better thermal performance than the best of the cavity model under the same thermal conditions for the same amount of the cavity and the fin volume. In addition, when Re number equals to the 10 and 400, the best fin model has 89.67% and 79.33% greater performance than the no fin and cavity model, respectively. It shows that the parallel flow case is less effected by the change of Re number relative to the cross-flow case. Finally, the peak temperature region appears at the outlet plane of the cylinder for the both models. Because, convective heat transfer weakens throughout the heat generating cylinder of the 3-dimensional model.

Overall, this study documents the heat transfer rate can be enhanced with cavities and/or fins. There is a best performing design for a given set of flow type, constraints and assumptions. This result is in accord with the Constructal law.

REFERENCES

1. E. Cetkin, Inverted fins for cooling of a non-uniformly heated domain. Journal of Thermal Engineering, **1**(2015), 1-9.

2. E. Cetkin, and A. Oliani, The natural emergence of asymmetric tree-shaped pathways for cooling of a non-uniformly heated domain. Journal of Applied Physics, 118 (2015), 024902.

3. A. Bejan, and S. Lorente, Design with Constructal Theory, 2008, Hoboken, New Jersey.

4. A. Bejan, Constructal-theory network of conducting paths for cooling a heat generating volume. International Journal of Heat and Mass Transfer, 1997. 40 (1997), 799-816.

5. A. Bejan, Advanced Engineering Thermodynamics. 2016, John Wiley & Sons, Hoboken, New Jersey.

6. A. Bejan, Shape and structure, from engineering to nature, Cambridge university press, 2000.

7. Reis, A.H., A.F. Miguel, and M. Aydin, Constructal theory of flow architecture of the lungs. Medical physics, 31 (2004), 1135-1140.

8. E.Cetkin, Three-dimensional high-conductivity trees for volumetric cooling, International Journal of Energy Research, 38 (2014), 1571-1577.

9. L.A.O. Rocha, S. Lorente, and A. Bejan, Conduction tree networks with loops for cooling a heat generating volume, International Journal of Heat and Mass Transfer, 49 (2006), 2626-2635.

10. A. Bejan and M. Almogbel, Constructal T-shaped fins. International Journal of Heat and Mass Transfer, 43 (2000), 2101-2115.

11. G. Lorenzini and S. Moretti, A CFD application to optimize T-shaped fins: comparisons to the constructal theory's results, Journal of Electronic Packaging, 129 (2007), 324-327.

12. S.A Hazarika, D. Bhanja, S. Nath, B. Kundu, Analytical solution to predict performance and optimum design parameters of a constructal T-shaped fin with simultaneous heat and mass transfer, Energy, 84 (2015), 303-316.

13. G. Lorenzini, C. Biserni, R.L. Correa, E.D. dos Santos, L.A. Isoldi, L.A.O Rocha, Constructal design of T-shaped assemblies of fins cooling a cylindrical solid body, International Journal of Thermal Sciences, 83 (2014), 96-103.

14. G. Lorenzini and L.A. O. Rocha, Constructal design of Y-shaped assembly of fins. International Journal of Heat and Mass Transfer, 49 (2006), 4552-4557.

15. G. Lorenzini and L.A.O. Rocha, Constructal design of T–Y assembly of fins for an optimized heat removal, International Journal of Heat and Mass Transfer, 52 (2009), 1458-1463.

16. G. Lorenzini, R.L Corrêa, E.D. dos Santos, L.A.O. Rocha, Constructal design of complex assembly of fins. Journal of Heat Transfer, 133 (2011), 081902.

17. L.A. Rocha, E. Lorenzini, and C. Biserni, Geometric optimization of shapes on the basis of Bejan's Constructal theory, International communications in heat and mass transfer, 32 (2005), 1281-1288.

18. Z. Xie, L. Chen, and F. Sun, Geometry optimization of T-shaped cavities according to constructal theory, Mathematical and Computer Modelling, 52 (2010), 1538-1546.

19. C.Biserni, L. Rocha, and A. Bejan, Inverted fins: geometric optimization of the intrusion into a conducting wall. International Journal of Heat and Mass Transfer, 47 (2004), 2577-2586.

20. G. Lorenzini, C. Biserni, E.D. Estrada, L.A. Isoldi, E.D. dos Santos, L.A.O. Rocha, Constructal design of convective Y-shaped cavities by means of genetic algorithm. Journal of Heat Transfer, 136 (2014), 071702.

21. G. Lorenzini and L.A.O. Rocha, Geometric optimization of TY-shaped cavity according to constructal design, International Journal of heat and mass transfer, 52 (2009), 4683-4688.

22. G. Lorenzini, F.L. Garcia, E.D. dos Santos, C. Biserni, L.A.O. Rocha, Constructal design applied to the optimization of complex geometries: TY-shaped cavities with two additional lateral intrusions cooled by convection, International Journal of Heat and Mass Transfer, 55 (2012), 1505-1512.

23. G. Lorenzini, E.S.D. Estrada, E.D. dos Santos, L.A. Isoldi, L.A.O. Rocha, Constructal design of convective cavities inserted into a cylindrical solid body for cooling, International Journal of Heat and Mass Transfer, 83 (2015), 75-83.

24 C. Biserni, L.A.O. Rocha, G. Stanescu, E. Lorenzini, Constructal H-shaped cavities according to Bejan’s theory, International Journal of Heat and Mass Transfer, 50 (2007), 2132-2138.

25. E. Cetkin, Constructal vascular structures with high-conductivity inserts for self cooling, Journal of Heat Transfer, 137 (2015), 111901.

26. COMSOL Multiphysics 5.0, COMSOL Inc., 2014.